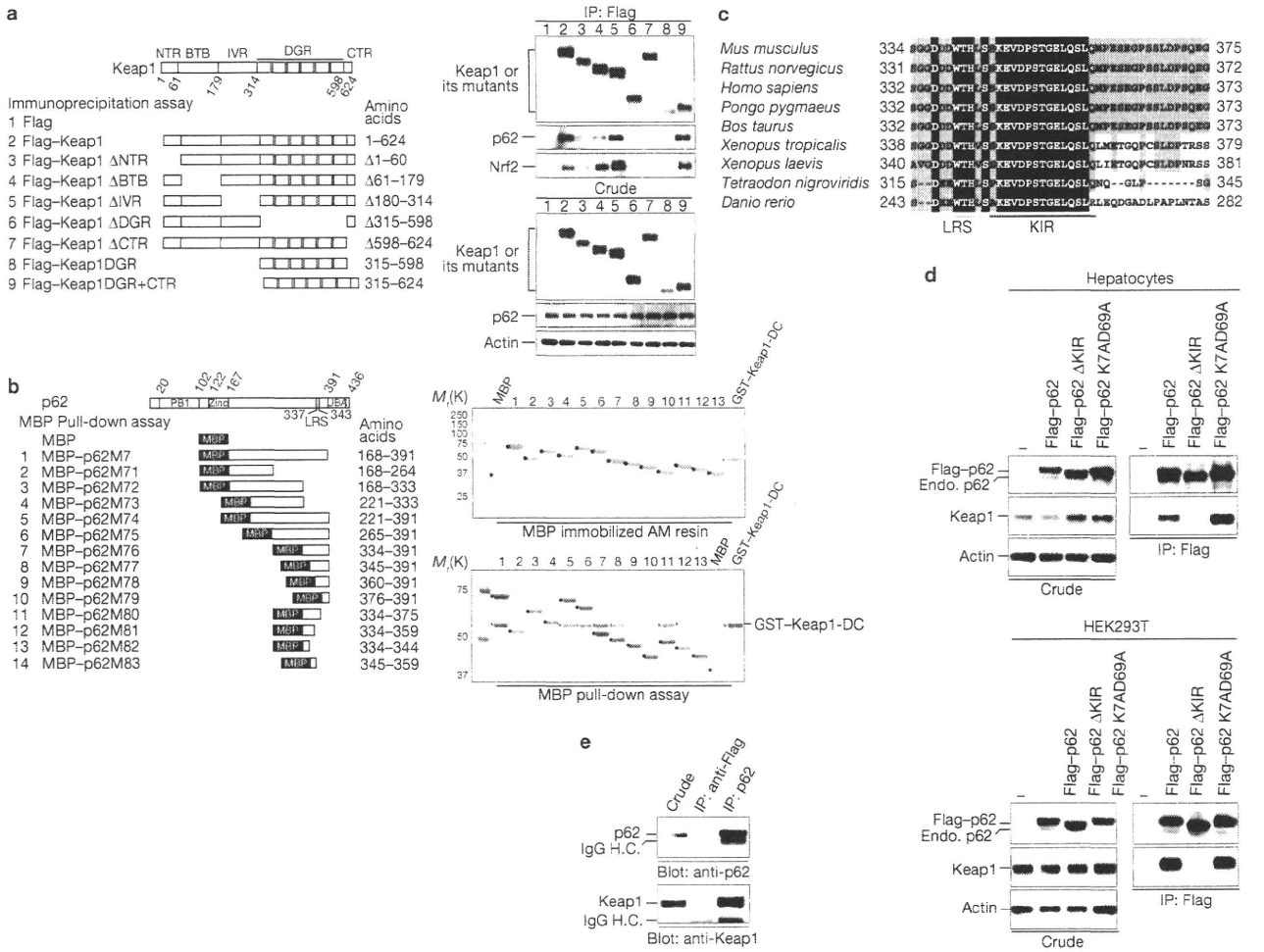

Figure 1 Interaction between Keap1 and p62. (**a**) Diagrams of the deletion–mutation constructs of Keap1 (left) and the corresponding immunoprecipitation assays (right). Each Flag-tagged mouse Keap1 and mutant was expressed in HEK293T cells. At 22 h after transfection, lysates were prepared and immunoprecipitated with anti-Flag antibody. The resulting immunoprecipitates were subjected to SDS–PAGE and analysed by immunoblotting with anti-Flag, anti-p62, anti-Nrf2 and anti-actin antibodies. Data are representative of three individual experiments. (**b**) Diagrams of the deletion–mutation constructs of p62 (left) and the corresponding input (upper right) and pull-down assay (lower right). The MBP-tagged mouse p62 deletion mutants conjugated to amylose (AM) resins were incubated with purified GST-tagged mouse Keap1-DC. The pulled-down complexes with the MBP–p62 mutants were subjected to SDS–PAGE and revealed by staining with Coomassie brilliant blue. The bands corresponding to MBP–p62 and its mutants are indicated by black dots. Red arrowheads indicate the band corresponding to GST–Keap1-DC. For details of construct 14 see Supplementary Information, Fig. S3. (**c**) Alignment of the Keap1-interacting regions (KIR; red line) and the LC3-recognition sequences (LRS; green line) of p62 homologues in various species. Black and grey boxes indicate identical amino acid residues with complete and partial conservation, respectively. (**d**) Immunoprecipitation assays. Flag-tagged p62, KIR-deleted p62 (p62 ΔKIR) and a p62 mutant defective in oligomerization (p62 K7AD69A) were expressed in primary mouse hepatocytes by the adenovirus system (left) or in HEK293T cells by transfection (right). Cell lysates were immunoprecipitated with anti-Flag antibody. The resulting immunoprecipitates were subjected to SDS–PAGE and analysed by immunoblotting with anti-p62 and anti-Keap1 antibodies. The bands corresponding to Flag–p62, endogenous p62, Keap1 and actin are indicated. The data shown are representative of three separate experiments. (**e**) Interaction of endogenous p62 with Keap1. Lysates prepared from the human hepatocellular carcinoma cell line Huh-1 were immunoprecipitated with anti-p62 antibody or anti-Flag antibody (negative control) followed by immunoblotting with antibodies against p62 and Keap1. The bands corresponding to endogenous p62, Keap1 and IgG heavy chain (IgG H.C.) are indicated. The data shown are representative of three separate experiments. Uncropped images of blots are shown in Supplementary Information, Fig. S11.

(kelch-like ECH-associated protein 1) is an adaptor of the ubiquitin ligase complex[24–27]. Exposure to electrophiles, reactive oxygen species and nitric oxide instigates the modification of the cysteine residues of Keap1, leading to its inactivation[28–30]. As a result, Nrf2 becomes stabilized and translocates to the nucleus to induce the transcription of numerous cytoprotective genes through its heterodimerization with small Maf proteins[31–33] (see Supplementary Information, Fig. S10). In this study we found that p62 acts to stabilize Nrf2 in autophagy-deficient mouse livers and subsequently induces the expression of various cytoprotective enzymes. This sustained activation of Nrf2 seems to be a major cause of toxicity in autophagy-impaired livers.

RESULTS

Identification of Keap1 as a p62-interacting protein

Previous genetic studies on the autophagy-essential protein Atg7 in the mouse showed that loss of autophagy caused a marked accumulation

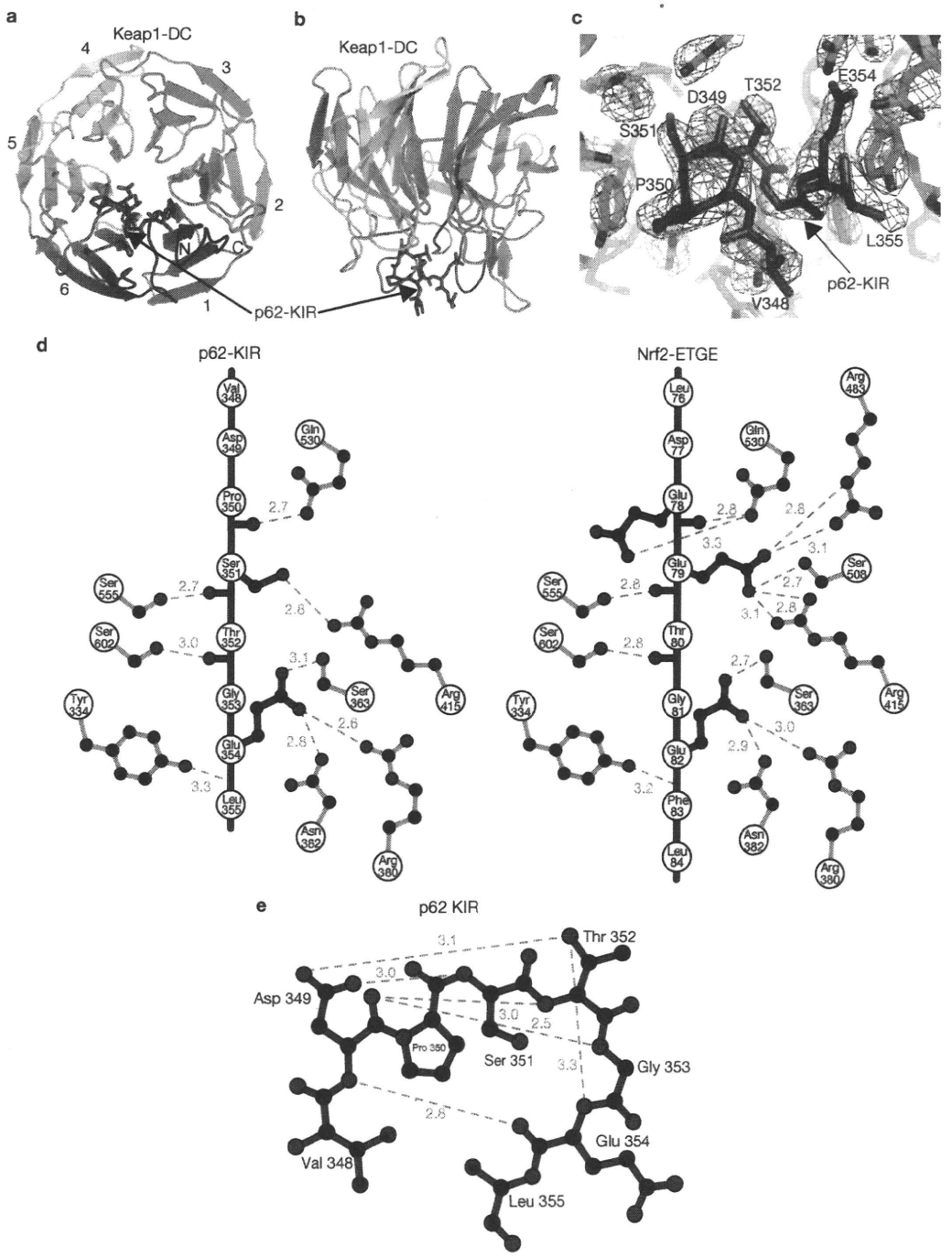

Figure 2 Crystal structure of Keap1-DC in complex with p62-KIR. (**a**, **b**) Bottom view (**a**) and side view (**b**) of the complex structure. The ribbon model represents Keap1-DC and the stick model shows p62-KIR. Each β-propeller blade is numbered from 1 to 6. (**c**) The simulated-annealing $F_o - F_c$ omit map is contoured at 3 σ. p62-KIR (pink) was omitted from the calculation. The electron density of the peptide-bound region V348 to L355 of p62-KIR was unambiguously visible. (**d**) Intermolecular hydrogen bonds of Keap1-DC in complex with p62-KIR (left; PDB ID 3ADE) and in complex with the Nrf2-ETGE region (right; PDB ID 1x2r). (**e**) Intra-peptide hydrogen bonds of p62-KIR in the Keap1-DC complex. Hydrogen bonds (green broken lines) and their distances (Å) are displayed in **d** and **e**.

of p62 along with robust induction of antioxidant proteins, including NAD(P)H dehydrogenase quinone 1 (Nqo1) and glutathione *S*-transferase (GST)[16]. A battery of such detoxifying and antioxidant genes is regulated by the transcription factor Nrf2, which is activated by oxidative and electrophilic stresses[31,32] (see Supplementary Information, Fig. S10). A prominent accumulation of Nrf2 in the nucleus was observed in livers deficient in Atg7, but this was ameliorated by the additional loss of p62 (ref. 16). We therefore postulated that in autophagy-deficient livers, oxidative stresses occur in a p62-dependent manner. However, treatment of *Atg7*-deficient hepatocytes with the antioxidant reagent *N*-acetylcysteine did not affect the nuclear accumulation of Nrf2 or the high-level expression of antioxidant enzymes (Supplementary

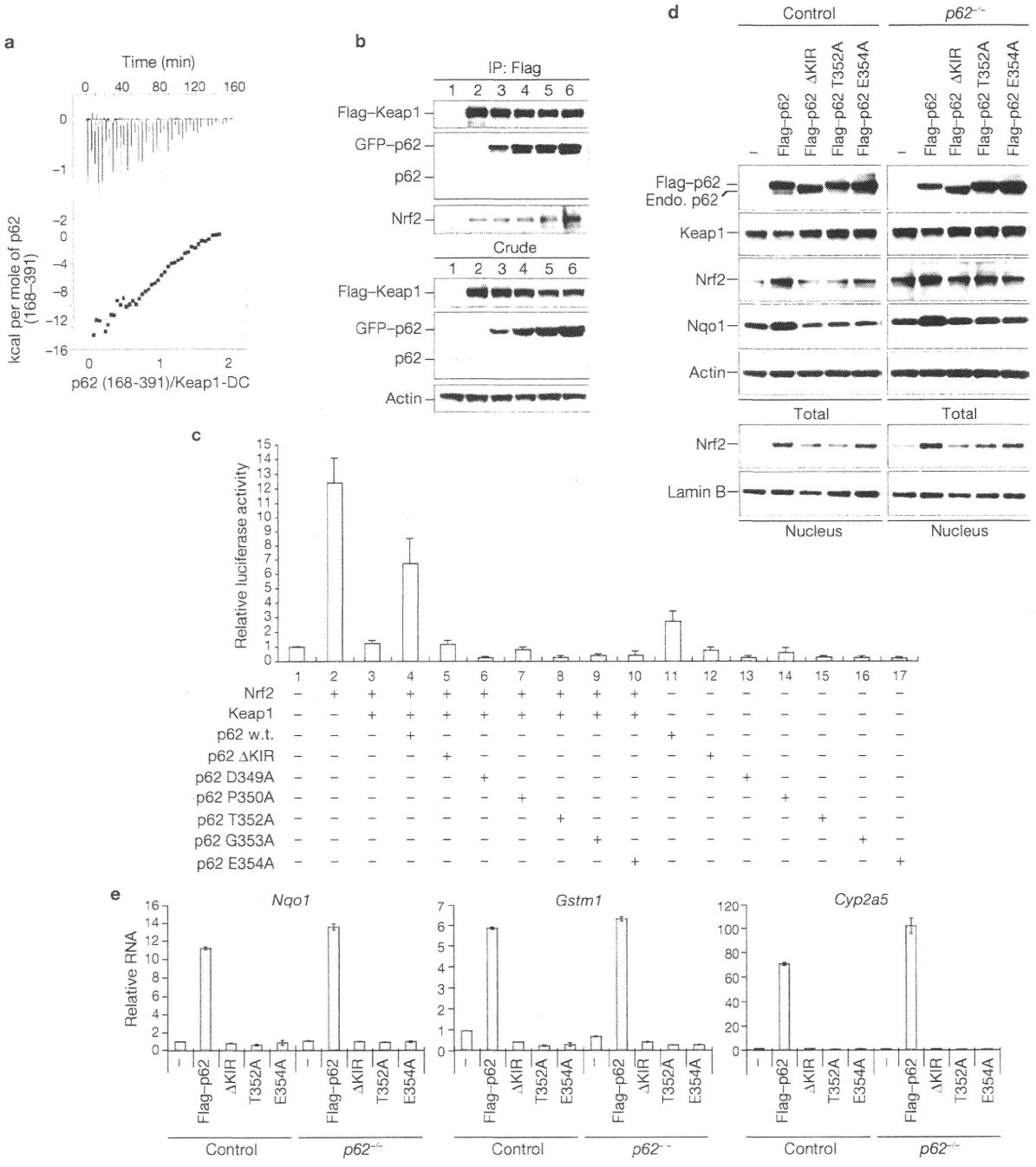

Figure 3 Competitive inhibition of the Nrf2–Keap1 pathway by p62. (**a**) A representative ITC profile of the titration of Keap1-DC with p62M7 (residues 168–391). The upper panel shows the raw ITC thermograms and the lower panel shows the fitted binding isotherms. (**b**) Immunoprecipitation assays. Flag-tagged Keap1 was co-expressed with increasing concentrations of green fluorescent protein (GFP)–p62 (lanes 3–6) in HEK293T cells. Cell lysates were immunoprecipitated with anti-Flag antibody. The resulting immunoprecipitates were subjected to SDS–PAGE and analysed by immunoblotting with anti-Flag, anti-p62 and anti-Nrf2 antibodies. The bands corresponding to Flag–Keap1, endogenous p62, Nrf2 and actin are indicated. Data are representative of three independent experiments. (**c**) The competitive p62 activity against Keap1 was measured by luciferase assay. The expression plasmids for Nrf2, Keap1 and p62 wild-type (w.t.) or its mutants were transfected into Hepa1 cells along with pNqo1-ARE reporter plasmid and pRL-TK as an internal control. At 36 h after transfection, the luciferase activity was measured in accordance with the instructions provided by the manufacturer. Assays were performed twice in triplicate. Data are means and s.d. for six determinations. (**d**) Immunoblot analysis. Flag-tagged p62 and its mutants defective in interacting with Keap1 were overproduced in wild-type and *p62*$^{-/-}$ primary mouse hepatocytes by the adenovirus system. At 48 h after infection, total cell lysates and nuclear fractions were prepared and subjected to immunoblot analysis with the antibodies specified. The bands corresponding to Flag–p62, endogenous p62, Keap1, Nrf2, Nqo1, actin and Lamin B are shown. Data are representative of three independent experiments. Uncropped images of blots are shown in Supplementary Information, Fig. S11. (**e**) Quantification of mRNA levels of the detoxification enzymes Nqo1, Gstm1 and Cyp2a5 in hepatocytes overexpressing Flag–p62 and its mutants. Total RNAs were prepared from non-infected or infected hepatocytes and reverse transcribed into their respective cDNAs, which were used as templates in real-time PCR analysis. Values were normalized to the amount of each mRNA in the non-infected hepatocytes. The experiments were performed three times. Data are means ± s.d. for three experiments.

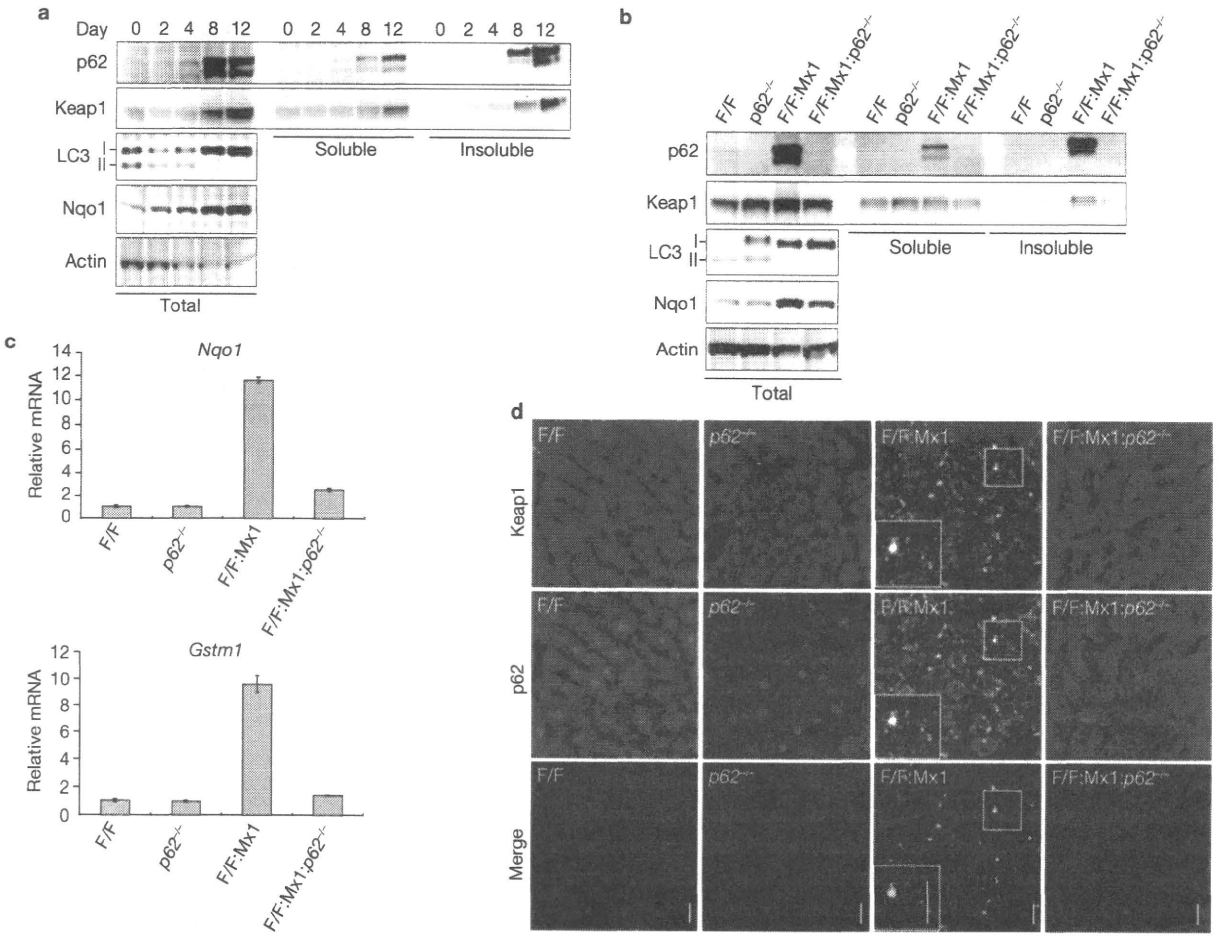

Figure 4 Formation of p62-positive and Keap1-positive inclusions in autophagy-deficient hepatocytes. (**a**) Insolubilization of Keap1 in *Atg7*-deficient hepatocytes. Liver homogenates from *Atg7*$^{F/F}$:Mx1 mice on various days after injection of poly(I)•poly(C) were separated into detergent-soluble and detergent-insoluble fractions with 0.5% Triton X-100. Each fraction was subjected to SDS–PAGE and analysed by immunoblotting with the indicated antibodies. The data displayed are representative of three separate experiments. (**b**) Immunoblot analysis of *Atg7*-deficient (*Atg7*$^{F/F}$:Mx1; *Atg7*$^{F/F}$ shown here as F/F) and *Atg7 p62*-deficient (*Atg7*$^{F/F}$:Mx1:*p62*$^{-/-}$) livers. Liver homogenates from mice of the stated genotypes at 12 days after injection of poly(I)•poly(C) were separated into detergent-soluble and detergent-insoluble fractions. Each fraction was subjected to SDS–PAGE and analysed by immunoblotting with the indicated antibodies. *Atg7*$^{F/F}$ mice[2] in which Atg7 is efficiently expressed at a level similar to that in the wild-type mice were used as control. Data shown are representative of three separate experiments. Uncropped images of blots are shown in Supplementary Information, Fig. S11. (**c**) Quantitative real-time PCR analyses of Nqo1 and Gstm1 in mouse livers. Total RNAs were prepared from livers of the indicated genotypes at 12 days after injection of poly(I)•poly(C). Values were normalized to the amount of mRNA in *Atg7*$^{F/F}$ liver. Data are means ± s.d. for three experiments. (**d**) Immunofluorescence analysis of the cellular localization of p62 and Keap1. Liver sections from mice of the indicated genotypes at 28 days after injection of poly(I)•poly(C) were immunostained with anti-Keap1 (top) and anti-p62 (middle) antibodies. Bottom: merged images of Keap1 (green) and p62 (red). Each inset in the *Atg7*-deficient liver panels is a magnified image of the boxed region. Scale bars, 20 μm.

Information, Fig. S1), suggesting the existence of p62-dependent regulation of Nrf2.

To explore cellular regulation by p62, we used a proteomic approach[34] to screen for proteins that interact with p62, by using HEK293T cells expressing tagged p62 protein. Keap1 was identified as a p62-interacting protein (data not shown). In an independent experiment with RL34 cells expressing tagged Keap1 protein, we isolated p62 as a Keap1-associating protein (data not shown). Keap1 is a substrate adaptor protein for Cullin-3-type ubiquitin E3 ligase. Keap1 possesses four domains: the Broad complex, Tramtrack, and Bric-a-Brac (BTB, amino-acid residues 61–179); the intervening region (IVR, residues 180–314); the double glycine repeat or kelch repeat (DGR, residues 315–598); and the carboxy-terminal region (CTR, residues 599–624)[24–27] (Fig. 1a). The DGR and CTR domains are collectively called the DC domain. The BTB domain serves to dimerize Keap1, enabling ubiquitin conjugation onto specific lysine residues located within the Neh2 domain of Nrf2 (refs 35, 36). The IVR domain interacts with Cullin 3 to promote Nrf2 ubiquitylation[26], whereas the DC domain physically interacts with the Neh2 domain of Nrf2 (refs 36 37). To specify the regions of Keap1 essential for its interaction with p62, we performed an immunoprecipitation assay. Whereas Keap1 C-terminal deletion mutants (ΔDGR and ΔCTR) did not interact with either endogenous p62 or Nrf2, Keap1 amino-terminal deletion mutants (ΔNTR, ΔBTB and ΔIVR) interacted with both endogenous p62 and Nrf2, although with weaker affinities than wild-type Keap1 (Fig. 1a). The Keap1-DC domain, but not the DGR domain, bound to both p62 and Nrf2 (Fig. 1a). The CTR domain contributes to the structural fold of Keap1-DC, which is required for interaction with Nrf2 (ref. 38). These results therefore suggest that the six-bladed β-propeller structure of Keap1 is essential for its molecular recognition of p62, as is the case for Nrf2.

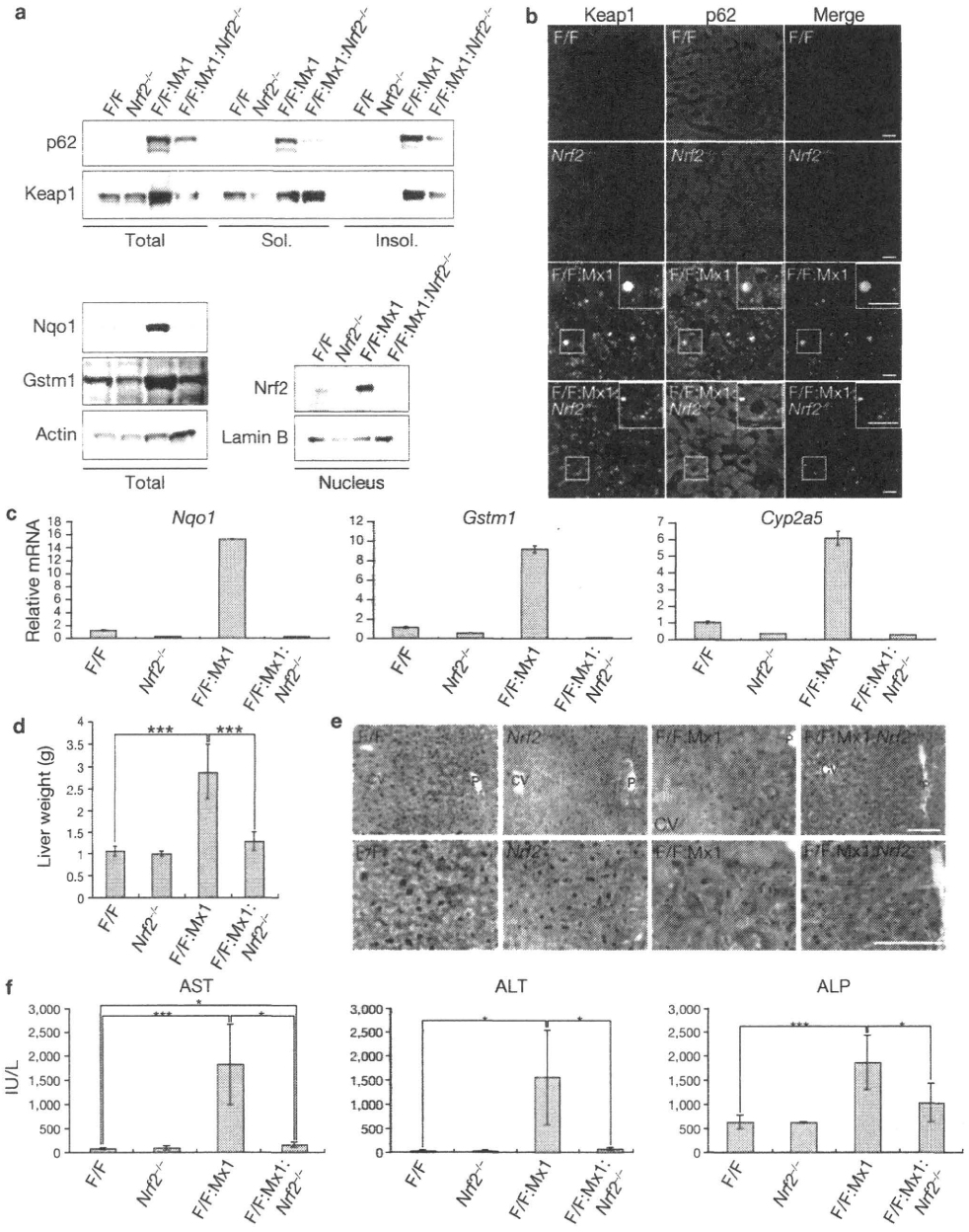

Figure 5 Amelioration of liver dysfunction in autophagy-deficient mice by the additional loss of *Nrf2*. (**a**) Immunoblotting of *Atg7*-deficient (*Atg7*$^{F/F}$:Mx1; *Atg7*$^{F/F}$ shown here as F/F) and *Atg7 Nrf2*-deficient (*Atg7*$^{F/F}$:Mx1:*Nrf2*$^{-/-}$) livers. Liver homogenates from mice of the assigned genotypes at 28 days after injection of poly(I)•poly(C) were separated into detergent-soluble and detergent-insoluble fractions. Total, soluble and insoluble fractions were subjected to SDS–PAGE and analysed by immunoblotting with the indicated antibodies (top section). Total lysates were subjected to SDS–PAGE and analysed by immunoblotting with antibodies against Nqo1, Gstm1 and actin (bottom left section). Nuclear fractions were prepared from the livers of the indicated genotypes at 28 days after injection of poly(I)•poly(C), subjected to SDS–PAGE and analysed by immunoblotting with antibodies against Nrf2 and Lamin B (as control) (bottom right section). Data were obtained from three independent experiments. Uncropped images of blots are shown in Supplementary Information, Fig. S11. (**b**) Immunofluorescence analysis of the cellular localization of p62 and Keap1. Liver sections from mice of the indicated genotypes at 28 days after injection of poly(I)•poly(C) were immunostained with anti-Keap1 (left) and anti-p62 (middle) antibodies. Right: merged images of Keap1 (green) and p62 (red). Each inset in the *Atg7*-deficient and *Atg7 Nrf2*-deficient liver panels is a magnified image of the boxed region. Scale bars, 20 μm. (**c**) Quantitative real-time PCR analyses of Nqo1, Gstm1 and Cy2a5 in mouse livers. Total RNAs were prepared from livers of the indicated genotypes at 28 days after injection of poly(I)•poly(C). Values were normalized to the amount of mRNA in the *Atg7*$^{F/F}$ liver. Data are means ± s.d. for three experiments. (**d**) Liver weight. The weights of the mouse livers of the different genotypes shown at 28 days after injection of poly(I)•poly(C) were measured. Data are means ± s.d. for five mice from each group. Three asterisks, $P < 0.001$ (Student's *t*-test). (**e**) Histological analysis of the mouse liver of the indicated genotypes. At 28 days after injection of poly(I)•poly(C), the livers were processed for haematoxylin/eosin staining. Higher-magnification views are shown in the bottom panels. CV, central vein; P, portal vein. Scale bars, 100 μm. (**f**) Liver function tests of the mice used in **d**. The serum levels of aspartate aminotransferase (AST), alanine aminotransferase (ALT) and alkaline phosphatase (ALP) were measured. (IU/L, international unit per liter). Data are means ± s.d. for seven mice from each group. Asterisk, $P < 0.05$; three asterisks, $P < 0.001$.

p62 comprises an N-terminal region that includes Phox and Bem1p (PB1) (residues 20–102) and a zinc finger (residues 122–167), a central region containing an LC3-recognition sequence (LRS) (residues 337–343), and a C-terminal region encompassing a ubiquitin-associated domain (UBA) (residues 391–436)[14,15,39] (Fig. 1b). To determine which domain of p62 is required for its interaction with Keap1, we divided p62 into three regions and employed a pull-down assay with the Keap1-DC domain (Supplementary Information, Fig. S2). The Keap1-DC domain was clearly detected in pull-down products both with full-length p62 and with p62M7, the p62 mutant harbouring the central region (residues 168–391). However, deletion mutants p62M3 and p62M5 showed a marked decrease in binding to the Keap1-DC domain (Supplementary Information, Fig. S2). To delineate the interaction domain more precisely, we prepared a deletion series of p62M7 (M71–M83) and performed the pull-down assay (Fig. 1b; Supplementary Information, Fig. S3a). These assays revealed that p62M83, covering residues 345–359, is essential and sufficient for the interaction between p62 and Keap1-DC (Supplementary Information, Fig. S3a). We therefore named residues 346–359 in p62M83 the Keap1-interacting region (KIR). KIR is located close to the C terminus of the LRS and is conserved across species (Fig. 1c). To further verify the Keap1–p62 interaction *in vivo*, we performed an immunoprecipitation assay. In primary mouse hepatocytes and HEK293T cells, endogenous Keap1 co-immunoprecipitated with wild-type Flag-tagged p62 and a mutant defective in oligomerization (p62 K7AD69A)[40], but failed to co-immunoprecipitate with KIR-deleted Flag–p62 (p62 ΔKIR) (Fig. 1d). The interaction between endogenous p62 and Keap1 was also verified (Fig. 1e).

Crystal structure of Keap1-DC in complex with p62-KIR

To delineate how Keap1 interacts with p62-KIR, we determined the crystal structure of Keap1-DC (residues 309–624) in complex with the p62-KIR peptide covering residues 346–359 at a resolution of 2.8 Å. Keap1-DC forms a six-bladed β-propeller structure with pseudo six-fold symmetry[37,38]. The KIR peptide binds to the bottom side of the β-propeller structure (Fig. 2a, b). A simulated-annealing $F_o - F_c$ omit map clearly indicated the electron density in the peptide bound region, in which 8 residues (V348 to L355) out of 14 were visible in p62-KIR, except for the L355 side chain (Fig. 2c).

Nrf2 is turned over rapidly through proteasomal degradation[24–27]. We previously identified the DLG and ETGE binding motifs present in the Neh2 domain of Nrf2, and these two motifs bind individually to the same binding pocket located at the bottom surface of Keap1 (refs 37, 38). One Nrf2 molecule binds to the Keap1 homodimer or to two Keap1 molecules. Because the two-site binding facilitates the ubiquitylation of lysine residues located between the DLG and ETGE motifs, the two-site substrate recognition mechanism is crucial for the rapid ubiquitylation of Nrf2 (refs 37, 38). Hydrogen-bond analysis revealed that the interactions between the Keap1-DC domain and p62-KIR (Fig. 2d, left) heavily overlap with the interactions between the Keap1-DC domain and Nrf2-ETGE (Fig. 2d, right). Eight amino-acid residues of Keap1-DC (Y334, S363, R380, N382, R415, Q530, S555 and S602) form hydrogen bonds with p62-KIR. These eight residues and two additional Keap1 residues (R483 and S508) are involved in Keap1 recognition of Nrf2-ETGE. These data strongly support the notion that p62-KIR binds to Keap1 in a manner very similar to that of the Nrf2-ETGE and Nrf2-DLG motifs[37,38].

The complex structure of Keap1-DC and p62-KIR showed that, of the eight amino-acid residues of the KIR domain, five residues (P350, S351, T352, E354 and L355) are involved in the interaction with Keap1 (Fig. 2d, left). To further verify this interaction biochemically, point mutations were created in the amino-acid residues of KIR in the mutant construct p62M80 by alanine replacement (Supplementary Information, Fig. S3a). A pull-down assay revealed that formation of the Keap1-DC–p62M80 complex was significantly decreased in the D349A, P350A, T352A, G353A and E354A mutants (Supplementary Information, Fig. S3a). Consistent with this experiment, immunoprecipitation analysis also revealed that these mutants showed a marked decrease in binding to Keap1 (Supplementary Information, Fig. S3b). The S351A mutation did not affect binding to Keap1 in either experiment, in spite of the direct interaction between S351 and Keap1 (Fig. 2d, left). The D349A mutation significantly inhibited the interaction with Keap1 (Supplementary Information, Fig. S3b), even though D349 does not interact directly with Keap1 (Fig. 2d, left). Residue D349 is involved in intra-peptide hydrogen bonding with S351 and T352, which stabilizes the type I β-turn in p62-KIR (Fig. 2e); this seems to be critical for the interaction between Keap1-DC and p62-KIR.

Because the tertiary structure of the complex indicates that p62-KIR associates with eight amino-acid residues in the basic surface of Keap1-DC, we introduced mutations in the residues of Keap1-DC (Y334, S363, R380, N382, R415, S508, Q530, S555 and S602) that are critical in the interaction with the KIR domain, and executed a GST pull-down assay (Supplementary Information, Fig. S3c). All except one of these GST–Keap1-DC mutants were markedly impaired in their ability to pull down maltose-binding protein (MBP)–p62M80 (Supplementary Information, Fig. S3c); the exception was R483A, which is not involved in the interaction with KIR (Fig. 2d). Further immunoprecipitation analysis confirmed that these residues in Keap1 are essential for efficient interaction with endogenous p62 and Nrf2 (Supplementary Information, Fig. S3d). These biochemical results are in good agreement with the crystal structure analysis.

Competitive inhibition of the Nrf2–Keap1 pathway by p62

Previous structural and kinetics studies demonstrated that the ETGE motif has a high affinity but the DLG motif has a low affinity for the same basic surface of Keap1 ($K_{a,ETGE} = (1.90 \pm 0.40) \times 10^8\ M^{-1}$, compared with $K_{a,DLG} = (1.00 \pm 0.00) \times 10^6\ M^{-1}$) (ref. 41). If the affinity of the p62 KIR domain for the basic surface in Keap1 were higher than or comparable to that of the ETGE or DLG motif, p62 might serve as an endogenous protein inducer of Nrf2 target genes by competitive binding inhibition of the Nrf2–Keap1 complex. It was therefore important to determine the binding-dissociation constant of Keap1–p62. Assessment of the binding energy by isothermal titration calorimetry (ITC) showed that the affinity of p62M7 (residues 168–391) for Keap1-DC ($K_a = (5.4 \pm 0.3) \times 10^5\ M^{-1}$) was similar to that of the DLG motif (Fig. 3a) and that, unlike with Nrf2, the binding stoichiometry was 1:1. This result suggests that overproduction of p62 counteracts the interaction between Nrf2-DLG and Keap1, but not that between Nrf2-ETGE and Keap1. In support of this notion, whereas the amounts of p62 forming a complex with Flag–Keap1 increased in proportion to the p62 expression level, the levels of Nrf2 interacting with Keap1 were hardly affected by overexpression of p62 (Fig. 3b). Meanwhile, p62 overproduction led to a marked decrease in Nrf2 ubiquitylation (see Supplementary Information, Fig. S4) and consequent Nrf2 stabilization (see Fig. 3d), suggesting that p62 inhibits Nrf2-DLG, but not Nrf2-ETGE, from interacting with Keap1.

So far, structural and kinetic analyses have strongly argued that p62 competitively inhibits the Keap1–Nrf2 interaction, leading to

the stabilization of Nrf2 and the expression of cytoprotective genes. To verify this concept further, we performed luciferase assays with a reporter plasmid harbouring the canonical Nrf2 recognition motif referred to as the ARE (antioxidant-responsive element). The transactivation activity of Nrf2 was suppressed by simultaneous expression of Keap1 (Fig. 3c, lanes 2 and 3), but this repression by Keap1 was inhibited by overexpression of p62 (Fig. 3c, lane 4). Mutants of p62 defective in interaction with Keap1 failed to counteract the repression of Nrf2 activity by Keap1 (Fig. 3c, lanes 5–10). Even in the absence of Keap1 transfection, p62 overexpression activated reporter gene expression (Fig. 3c, lane 11), perhaps by targeting the interaction of endogenous Keap1 with Nrf2; however, p62 mutants did not show this activity (Fig. 3c, lanes 12–17). This antagonistic effect of p62 to Keap1 seems to be independent of the self-oligomerization ability of p62 because the oligomerization-defective mutant p62 K7AD69A similarly counteracted the repression by Keap1 (Supplementary Information, Fig. S5a).

To examine whether p62 overexpression reinforces Nrf2 stability, we infected wild-type and *p62*$^{-/-}$ mouse primary hepatocytes with adenovirus Flag-tagged wild-type p62 and p62 mutants (ΔKIR, T352A and E354A) severely attenuated in their interactions with Keap1 (see Fig. 1d for ΔKIR; see Supplementary Information, Fig. S3a, b, for T352A and E354A). In both wild-type and mutant hepatocytes, overproduction of Flag–p62, but not of the mutants, triggered an increase in both total Nrf2 (Fig. 3d, upper panel) and the level of Nrf2 in the nuclear fractions (Fig. 3d, lower panel; Supplementary Information, Fig. S6). Because overproduction of Flag–p62, but not of the mutants, in primary mouse hepatocytes significantly inhibited Nrf2 ubiquitylation (Supplementary Information, Fig. S4), the Nrf2 stabilization can be attributed to Nrf2 being outcompeted by p62 for Keap1 binding. Consistent with this conclusion, the expression of Nrf2 target genes, such as *Nqo1*, *Gstm1* and *Cyp2a5*, was induced by the expression of Flag–p62, but not by expression of the mutants deficient in interaction with Keap1 (Fig. 3d, e; Supplementary Information, Fig. S6). In contrast, another p62 mutant (K7AD69A), which was defective in self-oligomerization but able to interact with Keap1 (see Fig. 1d) activated Nrf2 target genes to a modest but significant extent (Supplementary Information, Fig. S5b, c).

Keap1 is sequestered in inclusion bodies in a p62-dependent manner

The next series of experiments served to clarify whether the Nrf2–Keap1 interaction is affected by the intracellular accumulation of p62 or p62-positive and ubiquitin-positive inclusion bodies, which is known to occur in autophagy-deficient liver[16]. These studies were conducted in *Atg7*$^{F/F}$:Mx1 mice in which *Atg7* can be depleted in the liver by intraperitoneal injection of polyinosinic acid•polycytidylic acid (poly(I)•poly(C))[2]. Consistent with our previous work[16], immunoblot analysis revealed that p62 started to accumulate at day 4, was abundant in both the detergent-soluble and insoluble fractions at day 8 and further increased in both fractions at day 12 after injection of poly(I)•poly(C) (Fig. 4a). This pattern correlated well with the decrease in conversion of LC3-I to LC3-II, which signifies defective autophagosome formation[42] (Fig. 4a). On accumulation of p62, Keap1 was detected abundantly, especially in the detergent-insoluble fraction (Fig. 4a). The quantity of Nqo1 also increased gradually in *Atg7*-deficient livers (Fig. 4a), suggesting that Keap1 was inactivated by the loss of autophagy.

To determine whether the accumulation of Keap1 in the insoluble fraction of autophagy-deficient livers depends on the presence of p62, we used *Atg7*:*p62*-double-knockout mice (*Atg7*$^{F/F}$:Mx1:*p62*$^{-/-}$ or *Atg7 p62* DKO)[16]. The concurrent loss of *Atg7* and *p62* in the liver significantly suppressed the accumulation of Keap1 in the insoluble fraction that was observed in *Atg7*-deficient livers (Fig. 4b). This indicates that Keap1 is inactivated in a p62-dependent manner. Indeed, the high mRNA and protein levels of Nrf2 target genes in *Atg7*-deficient livers returned to almost normal levels after the additional loss of p62 (Fig. 4b, c). Immunofluorescence microscopy showed that the numerous Keap1-positive inclusions of various sizes seen in *Atg7*-deficient hepatocytes were absent from *Atg7 p62*-DKO hepatocytes (Fig. 4d). Double immunofluorescence microscopy showed that most of the Keap1-containing inclusions observed in *Atg7*-deficient hepatocytes were also positive for p62 (Fig. 4d). Taken together, these results indicate that under conditions of suppressed autophagy, a significant population of Keap1 is trapped by the excessive upsurge in p62, leading to sequestration of Keap1 into p62-positive and ubiquitin-positive inclusions.

Liver injury in autophagy-deficient mice is alleviated by loss of *Nrf2*

Although the excessive build-up of p62 seems to be the main cause of the pathogenic changes seen in the livers of autophagy-deficient mice, the molecular events involved in the pathogenic onset are still unknown. The data described so far suggest that p62-dependent regulation of the Nrf2–Keap1 pathway is involved in the pathological changes found in autophagy-deficient mice. To address this point, we crossed *Atg7*$^{F/F}$:Mx1 mice with *Nrf2*$^{-/-}$ mice[21] to produce *Atg7*:*Nrf2*-double-knockout mice (*Atg7*$^{F/F}$:Mx1:*Nrf2*$^{-/-}$ or *Atg7 Nrf2* DKO). Immunoblot analysis revealed that although the amount of p62 in *Atg7 Nrf2*-DKO livers was lower than that in *Atg7*-deficient livers, it was markedly higher than in control and *Nrf2*-knockout mouse livers (Fig. 5a). About half of the p62 in *Atg7 Nrf2*-DKO livers and *Atg7*-deficient livers was recovered in the insoluble fraction (Fig. 5a). The lower p62 level in *Atg7 Nrf2*-DKO mouse livers might be attributable, at least in part, to the loss of Nrf2 regulation for *p62* gene transcription[43]. Keap1 was also fractionated into the insoluble fraction in *Atg7*-deficient and *Atg7 Nrf2*-DKO mouse livers in proportion to the amount of insoluble p62 (Fig. 5a). The Keap1-positive aggregates detected in *Atg7*-deficient hepatocytes were also found in *Atg7 Nrf2*-DKO hepatocytes, although the aggregates were smaller and were almost completely co-localized with p62 (Fig. 5b). Electron microscopy showed accumulation of organelles and inclusion bodies in *Atg7 Nrf2*-DKO hepatocytes, similar to that observed in *Atg7*-deficient hepatocytes (Supplementary Information, Fig. S7). However, in contrast to *Atg7*-deficient livers, the induction of antioxidant proteins and detoxifying enzymes was completely abrogated in *Atg7 Nrf2*-DKO livers (Fig. 5a, c), confirming the Nrf2-dependent transcriptional induction of cytoprotective enzymes in autophagy-deficient livers.

We further examined the liver damage in these mice. Increased liver weight (Fig. 5d), disorganization of lobular structures (Fig. 5e, upper panels), hepatocytic hypertrophy (Fig. 5e, lower panels), an increased proportion of infiltrating cells (data not shown), and higher serum levels of aspartate aminotransferase, alanine aminotransferase and alkaline phosphatase (Fig. 5f) were observed in *Atg7*-deficient livers[2]; these were significantly suppressed by the additional loss of *Nrf2*. These results strongly suggest that persistent activation of Nrf2 in autophagy-deficient conditions may be one of the main causes of liver injury.

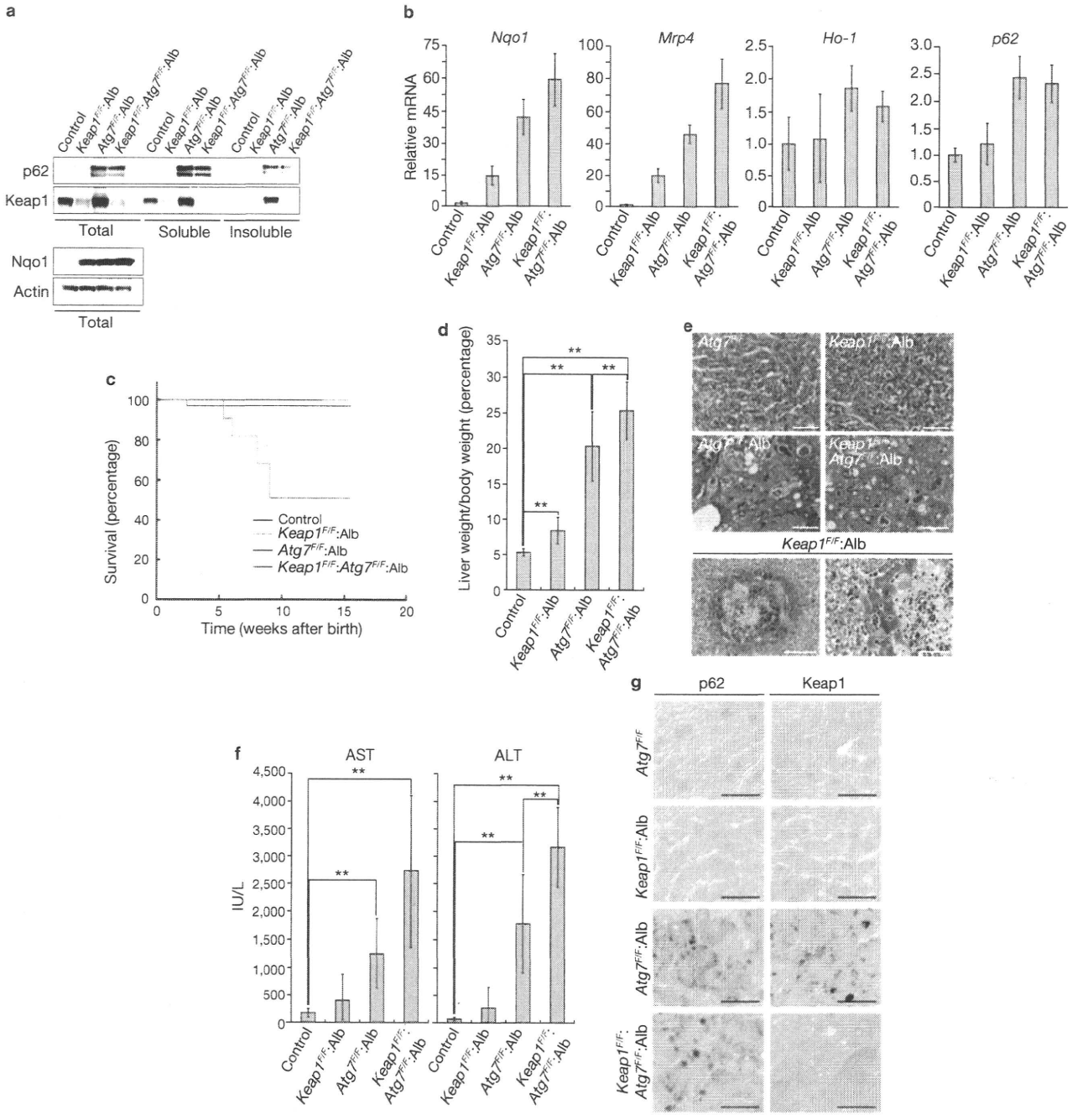

Figure 6 Exacerbation of liver dysfunction in autophagy-deficient mice by the additional loss of *Keap1*. (**a**) Immunoblotting of *Keap1*-deficient (*Keap1*$^{F/F}$:Alb) and *Keap1 Atg7*-deficient (*Keap1*$^{F/F}$:*Atg7*$^{F/F}$:Alb) livers. Liver homogenates from 8-week-old mice of these genotypes were separated into detergent-soluble and detergent-insoluble fractions. Total, soluble and insoluble fractions were subjected to SDS–PAGE and analysed by immunoblotting with the indicated antibodies (top section). Total lysates were subjected to SDS–PAGE and analysed by immunoblotting with antibodies against Nqo1 and actin (bottom section). Data were obtained from three independent experiments. Uncropped images of blots are shown in Supplementary Information, Fig. S11. (**b**) Quantitative real-time PCR analyses of Nqo1, Mrp4, p62 and Ho-1 in mouse livers. Total RNAs were prepared from livers of 9-week-old indicated genotypes. Values were normalized to the amount of mRNA in the *Atg7*$^{F/F}$ liver (control). Data are means ± s.d. for three experiments. (**c**) Kaplan–Meier curves of survival of *Atg7*$^{F/F}$:Alb and *Keap1*$^{F/F}$:*Atg7*$^{F/F}$:Alb mice. The survival analysis of control ($n = 33$), *Keap1*$^{F/F}$:Alb ($n = 15$), *Atg7*$^{F/F}$:Alb ($n = 12$) and *Keap1*$^{F/F}$:*Atg7*$^{F/F}$:Alb mice ($n = 14$) was based on a 16-week follow-up period. (**d**) Liver weight relative to body weight was measured for the different genotypes. Data are means ± s.d. for *Atg7*$^{F/F}$ (control) ($n = 24$), *Keap1*$^{F/F}$:Alb ($n = 13$), *Atg7*$^{F/F}$:Alb ($n = 9$) and *Keap1*$^{F/F}$:*Atg7*$^{F/F}$:Alb mice ($n = 7$). Two asterisks, $P < 0.01$ (Student's *t*-test). (**e**) Histological analysis of mouse liver of the indicated genotypes. The livers from 9-week-old mice were processed for haematoxylin/eosin staining. Scale bar, 50 μm (left bottom panel); 20 μm (other panels). (**f**) Liver function tests of the mice used in **d**. The serum levels of aspartate aminotransferase (AST) and alanine aminotransferase (ALT) were measured. Data are means ± s.d. for *Atg7*$^{F/F}$ (control) ($n = 24$), *Keap1*$^{F/F}$:Alb ($n = 13$), *Atg7*$^{F/F}$:Alb ($n = 9$) and *Keap1*$^{F/F}$:*Atg7*$^{F/F}$:Alb mice ($n = 7$). Two asterisks, $P < 0.01$. (**g**) Immunohistochemical analysis of cellular localization of p62 and Keap1. Paraffin sections of the liver from 9-week-old mice of the indicated genotypes were immunolabelled with anti-p62 (left) and anti-Keap1 (right) antibodies. Scale bars, 20 μm.

Liver injury in autophagy-deficient mice is exacerbated by loss of *Keap1*

To consolidate the notion that persistent activation of Nrf2 accompanied by defective autophagy causes liver injury, we generated hepatocyte-specific *Keap1*:*Atg7*-double-knockout mice (*Keap1*$^{F/F}$:*Atg7*$^{F/F}$:Alb or *Keap1 Atg7* DKO) by crossing *Keap1*$^{F/F}$:Alb[44] with *Atg7*$^{F/F}$ mice. *Keap1*-deficient mouse livers showed hyper-activation of Nrf2 (Fig. 6a, b), mild hepatomegaly (Fig. 6d) and occasional focal necrotic cell death (Fig. 6e, bottom panels), indicating that persistent activation of Nrf2 provokes cytotoxicity. Both the mRNA and protein levels of typical Nrf2 target genes in the *Keap1 Atg7*-DKO livers were significantly higher than those in single *Atg7*-knockout mouse livers (Fig. 6a, b), demonstrating that the loss of *Keap1* additively activates Nrf2 in autophagy-deficient livers. However, this additive effect was observed in only some Nrf2 target genes, such as *Nqo1* and *Mrp4*, but not in the other target genes, including those encoding p62 and haem oxygenase-1 (Ho-1) (Fig. 6a, b). Thus, transactivation by Nrf2 of certain Nrf2 target genes might be saturated in *Atg7*-deficient livers, so that levels of p62 and p62-positive aggregates in the *Keap1 Atg7*-DKO livers seemed to be similar to those in *Atg7*-deficient livers (Fig. 6a, g).

Although *Keap1 Atg7*-DKO mice were born at a Mendelian frequency, the survival rate of these mice diminished markedly 6 weeks after birth (Fig. 6c). We observed growth retardation at about 4 weeks (data not shown). Histological analysis showed pathological changes in DKO liver that were similar to those observed in *Atg7*-deficient liver: hepatocytic swellings and/or necrotic changes, appearance of acidophilic bodies, and cellular infiltration (Fig. 6e). The DKO mice showed increased liver weight (relative to body weight; Fig. 6d) and a high level of serum alanine aminotransferase (Fig. 6f) compared with *Atg7*-single-knockout mice. These results further support our conclusion that autophagy deficiency provokes deregulation of the Nrf2–Keap1 system and that constitutive activation of Nrf2 leads to hepatotoxicity.

DISCUSSION

In this study we have demonstrated that p62 serves as an endogenous protein inducer of Nrf2. We previously deciphered the unique association mechanism of Nrf2 and Keap1 in which two Keap1 molecules interact with one Nrf2 molecule through its DLG and ETGE motifs. This two-site binding facilitates the ubiquitylation and degradation of Nrf2 (refs 37, 38). This mechanism has been verified by the finding that, in cases of human lung cancer, somatic mutations in Nrf2 are located exclusively in the DLG and ETGE motifs[45]. We proposed the 'hinge and latch' model as the stress-sensing mechanism, by which the weak-affinity DLG motif acts as a latch for turning the ubiquitylation of Nrf2 on or off (refs 37, 41). Here we found that, on perturbation of autophagy, p62 accumulates and activates Nrf2 by competing with Nrf2 for its binding to Keap1. The following observations are significant: first, through its KIR motif, p62 interacts directly with Keap1; second, the binding mode of KIR is similar to that of Nrf2-ETGE or Nrf2-DLG, where it binds to the basic surface pocket at the bottom of Keap1; and third, p62-KIR binds to Keap1 with an affinity similar to that of Nrf2-DLG but much weaker than that of Nrf2-ETGE. It therefore seems most plausible that the KIR motif interferes directly with the binding of the DLG motif to Keap1. These results support our argument that the 'hinge and latch' mechanism actually operates *in vivo* (see the model in Supplementary Information, Fig. S10).

Our present study demonstrates that the pathological changes observed in autophagy-defective livers are due, at least in part, to persistent activation of Nrf2 by the excess accumulation of p62. This was an unexpected result because most Nrf2-dependent gene products retain cytoprotective function[31]. To verify this finding further, we performed a microarray analysis in *Atg7*-knockout and *Atg7 Nrf2*-DKO mouse livers. The analysis showed that more than 100 genes were activated in an Nrf2-dependent manner in autophagy-deficient livers, with a range of induction from 2-fold to as much as 100-fold (data not shown, and Fig. 5c). Furthermore, our comprehensive proteomics analysis reported previously[46] showed that the Nrf2 target gene products, such as Gst-m1 and Gst-p1, were prominent proteins in autophagy-deficient liver. Surprisingly, Gst-m1 constituted 7.69 ± 1.25% of the cytosolic proteins in *Atg7*-deficient livers (Supplementary Information, Fig. S8). Thus, the autophagy-deficient liver shows an abnormal accumulation of various Nrf2 target proteins. Because loss of *Keap1* in mouse hepatocytes resulted in only mild liver abnormality (Fig. 6d, e), the phenotypes detected in *Atg7*-deficient livers cannot be attributed solely to Nrf2 activation by loss of *Keap1*. It is therefore conceivable that the additional loss of autophagy greatly affects the development of liver abnormality. In other words, the collapse of the balance between the synthesis of cellular proteins (Nrf2-dependent robust protein synthesis) and their degradation (global turnover of cytoplasmic proteins through autophagy) could result in the appearance of destructive phenotypes (that is, hepatocytic hypertrophy due to the increased cellular protein volume followed by hepatomegaly and liver injury). In support of this conclusion, hepatocyte-specific *Keap1 Atg7*-DKO mice showing high-level Nrf2 activity exhibited more severe hepatomegaly and liver injury than the single *Atg7*-deficient mice (Fig. 6c–f).

It has been reported that p62 accumulation in growing cell lines leads to a decrease in the ubiquitin–proteasomal (UPS) flux[47], implying that the cytotoxicity of p62 operates through inhibition of the UPS flux. However, overproduction of p62 did not induce inhibition of the UPS flux in primary culture hepatocytes (data not shown), suggesting that p62 accumulation is not cytotoxic towards quiescent cells. In fact, forced overexpression of p62 in primary culture hepatocytes lacking both *Atg7* and *p62* activated the expression of Nrf2 target genes but did not induce cell death (Supplementary Information, Fig. S9). We surmise that the hepatic injury caused by the *Atg7* deficiency is not attributable to cell-autonomous failure but rather to disintegration of the liver tissue as a result of hypertrophy of the hepatocytes. Indeed, both narrowing of sinusoidal capillaries and abnormal morphology of bile canaliculi were evident in *Atg7*-deficient liver (Figs 5e and 6e), suggesting that severe cholestasis and/or haemostasis might be the main causes of the liver injury.

Accumulation of p62, and/or p62-positive inclusions, has been reported in human liver diseases such as hepatocellular carcinoma, alcoholic hepatitis and α_1-antitrypsin deficiency[20]. We propose that in such pathological conditions, the high levels of p62 associated with the suppression of autophagy might result in activation of Nrf2. Further analysis is needed to clarify the regulation or dysregulation of the Nrf2–Keap1 pathway in these human diseases. □

METHODS

Methods and any associated references are available in the online version of the paper at http://www.nature.com/naturecellbiology/

Note: Supplementary Information is available on the Nature Cell Biology website.

ACKNOWLEDGEMENTS

We thank T. Kouno and K. Endo (Tokyo Metropolitan Institute of Medical Science) for technical assistance, and the beamline staff at NW12 of PF-AR (Tsukuba, Japan) for technical help in data collection. We also thank A. Yamada, K. Kanno

and A. Yabashi (Fukushima Medical University School of Medicine) for their help in histological studies; J. Yanagisawa (Tsukuba University) and Y. Saeki (Tokyo Metropolitan Institute of Medical Science) for mass spectrometric analyses; Y. Kawatani (Tohoku University) for technical assistance in microarray analyses; and R. Kopito and B. E. Riley (Stanford University) and T. Mizushima and T. Kumanomidou (Nagoya University) for helpful discussion. *p62*-knockout mice were provided by T. Ishii (Tsukuba University). The Biomedical Research Core of Tohoku University Graduate School of Medicine provided DRI-CHEM 7000V (Fuji Film Corp.). This work was supported by grants from the Japan Science and Technology Agency (M.K.), the Ministry of Education, Science and Culture of Japan (M.K., K.T. and M.Y.) and the Targeted Proteins Research Program (H.K., K.T. and M.Y.).

AUTHOR CONTRIBUTIONS

M.K., K.T., I.U. and A.S. performed most of the experiments that characterized the knockout mice. I.U., Y.-S.S., Y.I. and A.K. performed the biochemical and cell biological experiments. Y.N. carried out microarray analyses. S.-i.I and T.N. performed mass spectrometric analyses. S.W. performed the histological and microscopic analyses. Structural and kinetics analyses were completed by H.K. and K.I.T. M.K., K.T. and M.Y. conceived the experiments. M.K., H.K., S.W., H.M., K.T. and M.Y. wrote the paper. E.K. and T.U. provided intellectual support. All authors discussed the results and commented on the manuscript.

COMPETING FINANCIAL INTERESTS

The authors declare no competing financial interests.

Published online at http://www.nature.com/naturecellbiology
Reprints and permissions information is available online at http://npg.nature.com/reprintsandpermissions/

1. Mizushima, N., Levine, B., Cuervo, A. M. & Klionsky, D. J. Autophagy fights disease through cellular self-digestion. *Nature* **451,** 1069–1075 (2008).
2. Komatsu, M. *et al.* Impairment of starvation-induced and constitutive autophagy in Atg7-deficient mice. *J. Cell Biol.* **169,** 425–434 (2005).
3. Ebato, C. *et al.* Autophagy is important in islet homeostasis and compensatory increase of beta cell mass in response to high-fat diet. *Cell Metab.* **8,** 325–332 (2008).
4. Jung, H. S. *et al.* Loss of autophagy diminishes pancreatic beta cell mass and function with resultant hyperglycemia. *Cell Metab.* **8,** 318–324 (2008).
5. Nakai, A. *et al.* The role of autophagy in cardiomyocytes in the basal state and in response to hemodynamic stress. *Nature Med.* **13,** 619–624 (2007).
6. Komatsu, M. *et al.* Loss of autophagy in the central nervous system causes neurodegeneration in mice. *Nature* **441,** 880–884 (2006).
7. Hara, T. *et al.* Suppression of basal autophagy in neural cells causes neurodegenerative disease in mice. *Nature* **441,** 885–889 (2006).
8. Yorimitsu, T. & Klionsky, D. J. Autophagy: molecular machinery for self-eating. *Cell Death Differ.* **12** (Suppl. 2), 1542–1552 (2005).
9. Rubinsztein, D. C. The roles of intracellular protein-degradation pathways in neurodegeneration. *Nature* **443,** 780–786 (2006).
10. Platta, H. W. & Erdmann, R. Peroxisomal dynamics. *Trends Cell Biol.* **17,** 474–484 (2007).
11. Zhang, J. & Ney, P. A. Role of BNIP3 and NIX in cell death, autophagy, and mitophagy. *Cell Death Differ.* **16,** 939-946 (2009).
12. Levine, B. & Deretic, V. Unveiling the roles of autophagy in innate and adaptive immunity. *Nature Rev. Immunol.* **7,** 767–777 (2007).
13. Bjorkoy, G. *et al.* p62/SQSTM1 forms protein aggregates degraded by autophagy and has a protective effect on huntingtin-induced cell death. *J. Cell Biol.* **171,** 603–614 (2005).
14. Pankiv, S. *et al.* p62/SQSTM1 binds directly to Atg8/LC3 to facilitate degradation of ubiquitinated protein aggregates by autophagy. *J. Biol. Chem.* **282,** 24131–24145 (2007).
15. Ichimura, Y. *et al.* Structural basis for sorting mechanism of p62 in selective autophagy. *J. Biol. Chem.* **283,** 22847–22857 (2008).
16. Komatsu, M. *et al.* Homeostatic levels of p62 control cytoplasmic inclusion body formation in autophagy-deficient mice. *Cell* **131,** 1149–1163 (2007).
17. Nezis, I. P. *et al.* Ref(2)P, the *Drosophila melanogaster* homologue of mammalian p62, is required for the formation of protein aggregates in adult brain. *J. Cell Biol.* **180,** 1065–1071 (2008).
18. Kuusisto, E., Salminen, A. & Alafuzoff, I. Ubiquitin-binding protein p62 is present in neuronal and glial inclusions in human tauopathies and synucleinopathies. *Neuroreport* **12,** 2085–2090 (2001).
19. Stumptner, C., Fuchsbichler, A., Heid, H., Zatloukal, K. & Denk, H. Mallory body — a disease-associated type of sequestosome. *Hepatology* **35,** 1053–1062 (2002).
20. Zatloukal, K. *et al.* p62 Is a common component of cytoplasmic inclusions in protein aggregation diseases. *Am J Pathol* **160,** 255–263 (2002).
21. Itoh, K. *et al.* An Nrf2/small Maf heterodimer mediates the induction of phase II detoxifying enzyme genes through antioxidant response elements. *Biochem. Biophys. Res. Commun.* **236,** 313–322 (1997).
22. Itoh, K. *et al.* Keap1 represses nuclear activation of antioxidant responsive elements by Nrf2 through binding to the amino-terminal Neh2 domain. *Genes Dev.* **13,** 76–86 (1999).
23. Wakabayashi, N. *et al.* Keap1-null mutation leads to postnatal lethality due to constitutive Nrf2 activation. *Nature Genet.* **35,** 238–245 (2003).
24. Cullinan, S. B., Gordan, J. D., Jin, J., Harper, J. W. & Diehl, J. A. The Keap1-BTB protein is an adaptor that bridges Nrf2 to a Cul3-based E3 ligase: oxidative stress sensing by a Cul3-Keap1 ligase. *Mol. Cell. Biol.* **24,** 8477–8486 (2004).
25. Furukawa, M. & Xiong, Y. BTB protein Keap1 targets antioxidant transcription factor Nrf2 for ubiquitination by the Cullin 3-Roc1 ligase. *Mol. Cell. Biol.* **25,** 162–171 (2005).
26. Kobayashi, A. *et al.* Oxidative stress sensor Keap1 functions as an adaptor for Cul3-based E3 ligase to regulate proteasomal degradation of Nrf2. *Mol. Cell. Biol.* **24,** 7130–7139 (2004).
27. Zhang, D. D., Lo, S. C., Cross, J. V., Templeton, D. J. & Hannink, M. Keap1 is a redox-regulated substrate adaptor protein for a Cul3-dependent ubiquitin ligase complex. *Mol. Cell. Biol.* **24,** 10941–10953 (2004).
28. Dinkova-Kostova, A. T. *et al.* Direct evidence that sulfhydryl groups of Keap1 are the sensors regulating induction of phase 2 enzymes that protect against carcinogens and oxidants. *Proc. Natl Acad. Sci. USA* **99,** 11908–11913 (2002).
29. Wakabayashi, N. *et al.* Protection against electrophile and oxidant stress by induction of the phase 2 response: fate of cysteines of the Keap1 sensor modified by inducers. *Proc. Natl Acad. Sci. USA* **101,** 2040–2045 (2004).
30. Kobayashi, A. *et al.* Oxidative and electrophilic stresses activate Nrf2 through inhibition of ubiquitination activity of Keap1. *Mol. Cell. Biol.* **26,** 221–229 (2006).
31. Motohashi, H. & Yamamoto, M. Nrf2–Keap1 defines a physiologically important stress response mechanism. *Trends Mol. Med.* **10,** 549–557 (2004).
32. Holtzclaw, W. D., Dinkova-Kostova, A. T. & Talalay, P. Protection against electrophile and oxidative stress by induction of phase 2 genes: the quest for the elusive sensor that responds to inducers. *Adv. Enzyme Regul.* **44,** 335–367 (2004).
33. Kobayashi, M. & Yamamoto, M. Nrf2–Keap1 regulation of cellular defense mechanisms against electrophiles and reactive oxygen species. *Adv. Enzyme Regul.* **46,** 113–140 (2006).
34. Komatsu, M. *et al.* A novel protein-conjugating system for Ufm1, a ubiquitin-fold modifier. *EMBO J.* **23,** 1977–1986 (2004).
35. Zipper, L. M. & Mulcahy, R. T. The Keap1 BTB/POZ dimerization function is required to sequester Nrf2 in cytoplasm. *J. Biol. Chem.* **277,** 36544–36552 (2002).
36. McMahon, M., Thomas, N., Itoh, K., Yamamoto, M. & Hayes, J. D. Dimerization of substrate adaptors can facilitate cullin-mediated ubiquitylation of proteins by a 'tethering' mechanism: a two-site interaction model for the Nrf2–Keap1 complex. *J. Biol. Chem.* **281,** 24756–24768 (2006).
37. Tong, K. I. *et al.* Different electrostatic potentials define ETGE and DLG motifs as hinge and latch in oxidative stress response. *Mol. Cell. Biol.* **27,** 7511–7521 (2007).
38. Padmanabhan, B. *et al.* Structural basis for defects of Keap1 activity provoked by its point mutations in lung cancer. *Mol. Cell* **21,** 689–700 (2006).
39. Seibenhener, M. L., Geetha, T. & Wooten, M. W. Sequestosome 1/p62 — More than just a scaffold. *FEBS Lett.* **581,** 175–179 (2007).
40. Lamark, T. *et al.* Interaction codes within the family of mammalian Phox and Bem1p domain-containing proteins. *J. Biol. Chem.* **278,** 34568–34581 (2003).
41. Tong, K. I. *et al.* Keap1 recruits Neh2 through binding to ETGE and DLG motifs: characterization of the two-site molecular recognition model. *Mol. Cell. Biol.* **26,** 2887–2900 (2006).
42. Kabeya, Y. *et al.* LC3, a mammalian homologue of yeast Apg8p, is localized in autophagosome membranes after processing. *EMBO J.* **19,** 5720–5728 (2000).
43. Ishii, T. *et al.* Transcription factor Nrf2 coordinately regulates a group of oxidative stress-inducible genes in macrophages. *J. Biol. Chem.* **275,** 16023–16029 (2000).
44. Okawa, H. *et al.* Hepatocyte-specific deletion of the *keap1* gene activates Nrf2 and confers potent resistance against acute drug toxicity. *Biochem. Biophys. Res. Commun.* **339,** 79–88 (2006).
45. Shibata, T. *et al.* Cancer related mutations in NRF2 impair its recognition by Keap1-Cul3 E3 ligase and promote malignancy. *Proc. Natl Acad. Sci. USA* **105,** 13568–13573 (2008).
46. Matsumoto, N. *et al.* Comprehensive proteomics analysis of autophagy-deficient mouse liver. *Biochem. Biophys. Res. Commun.* **368,** 643–649 (2008).
47. Korolchuk, V. I., Mansilla, A., Menzies, F. M. & Rubinsztein, D. C. Autophagy inhibition compromises degradation of ubiquitin–proteasome pathway substrates. *Mol. Cell* **33,** 517–527 (2009).

PINK1 stabilized by mitochondrial depolarization recruits Parkin to damaged mitochondria and activates latent Parkin for mitophagy

Noriyuki Matsuda,[1] Shigeto Sato,[2] Kahori Shiba,[3] Kei Okatsu,[1] Keiko Saisho,[1] Clement A. Gautier,[4] Yu-shin Sou,[1] Shinji Saiki,[2] Sumihiro Kawajiri,[2] Fumiaki Sato,[3] Mayumi Kimura,[1] Masaaki Komatsu,[1,5] Nobutaka Hattori,[2] and Keiji Tanaka[1]

[1]Laboratory of Frontier Science, Tokyo Metropolitan Institute of Medical Science, Setagaya-ku, Tokyo 156-8506, Japan
[2]Department of Neurology and [3]Research Institute for Diseases of Old Age, Juntendo University School of Medicine, Bunkyo-ku, Tokyo 113-8421, Japan
[4]Center for Neurologic Diseases, Brigham and Women's Hospital, Harvard Medical School, Boston, MA 02115
[5]Precursory Research for Embryonic Science and Technology, Japan Science and Technology Agency, Kawaguchi 332-0012, Japan

Parkinson's disease (PD) is a prevalent neurodegenerative disorder. Recent identification of genes linked to familial forms of PD such as *Parkin* and *PINK1* (*PTEN-induced putative kinase 1*) has revealed that ubiquitylation and mitochondrial integrity are key factors in disease pathogenesis. However, the exact mechanism underlying the functional interplay between Parkin-catalyzed ubiquitylation and PINK1-regulated mitochondrial quality control remains an enigma. In this study, we show that PINK1 is rapidly and constitutively degraded under steady-state conditions in a mitochondrial membrane potential–dependent manner and that a loss in mitochondrial membrane potential stabilizes PINK1 mitochondrial accumulation. Furthermore, PINK1 recruits Parkin from the cytoplasm to mitochondria with low membrane potential to initiate the autophagic degradation of damaged mitochondria. Interestingly, the ubiquitin ligase activity of Parkin is repressed in the cytoplasm under steady-state conditions; however, PINK1-dependent mitochondrial localization liberates the latent enzymatic activity of Parkin. Some pathogenic mutations of PINK1 and Parkin interfere with the aforementioned events, suggesting an etiological importance. These results provide crucial insight into the pathogenic mechanisms of PD.

Introduction

Parkinson's disease (PD) is a very common movement disorder characterized by dopaminergic neuronal loss. The majority of PD cases are sporadic; however, the discovery of genes linked to rare familial forms of this disease has provided important insight into the molecular mechanisms of disease pathogenesis (Moore et al., 2005; Hardy et al., 2006). In 2000, we and others found that dysfunction of an E3 ubiquitin ligase (Imai et al., 2000; Shimura et al., 2000; Zhang et al., 2000) termed Parkin causes autosomal recessive juvenile Parkinsonism (Kitada et al., 1998). Since then, a multitude of papers have been published, but the mechanism by which dysfunction of Parkin causes autosomal recessive juvenile Parkinsonism has largely remained obscure, and claims of pathogenicity remain controversial (Lim, 2007; Matsuda and Tanaka, 2010). In addition, *PINK1* (*PTEN-induced putative kinase 1*) was identified in 2004 as the gene responsible for another form of early-onset PD (Valente et al., 2004). PINK1 functions in mitochondrial maintenance, suggesting that mitochondrial integrity is another key factor in disease pathogenesis (Dodson and Guo, 2007; Schapira, 2008). Intriguingly, genetic studies using *Drosophila melanogaster* revealed that PINK1 and Parkin function in the same pathway, with PINK1 functioning upstream of Parkin (Clark et al., 2006; Park et al., 2006; Yang et al., 2006). Little is known about how PINK1

Correspondence to Noriyuki Matsuda: matsuda-nr@igakuken.or.jp; or Keiji Tanaka: tanaka-kj@igakuken.or.jp

Abbreviations used in this paper: CCCP, carbonyl cyanide m-chlorophenylhydrazone; MEF, mouse embryonic fibroblast; Mt-GFP, mitochondria-targeting GFP; PD, Parkinson's disease.

© 2010 Matsuda et al. This article is distributed under the terms of an Attribution–Noncommercial–Share Alike–No Mirror Sites license for the first six months after the publication date (see http://www.rupress.org/terms). After six months it is available under a Creative Commons License (Attribution–Noncommercial–Share Alike 3.0 Unported license, as described at http://creativecommons.org/licenses/by-nc-sa/3.0/).

The Rockefeller University Press $30.00
J. Cell Biol. Vol. 189 No. 2 211–221
www.jcb.org/cgi/doi/10.1083/jcb.200910140

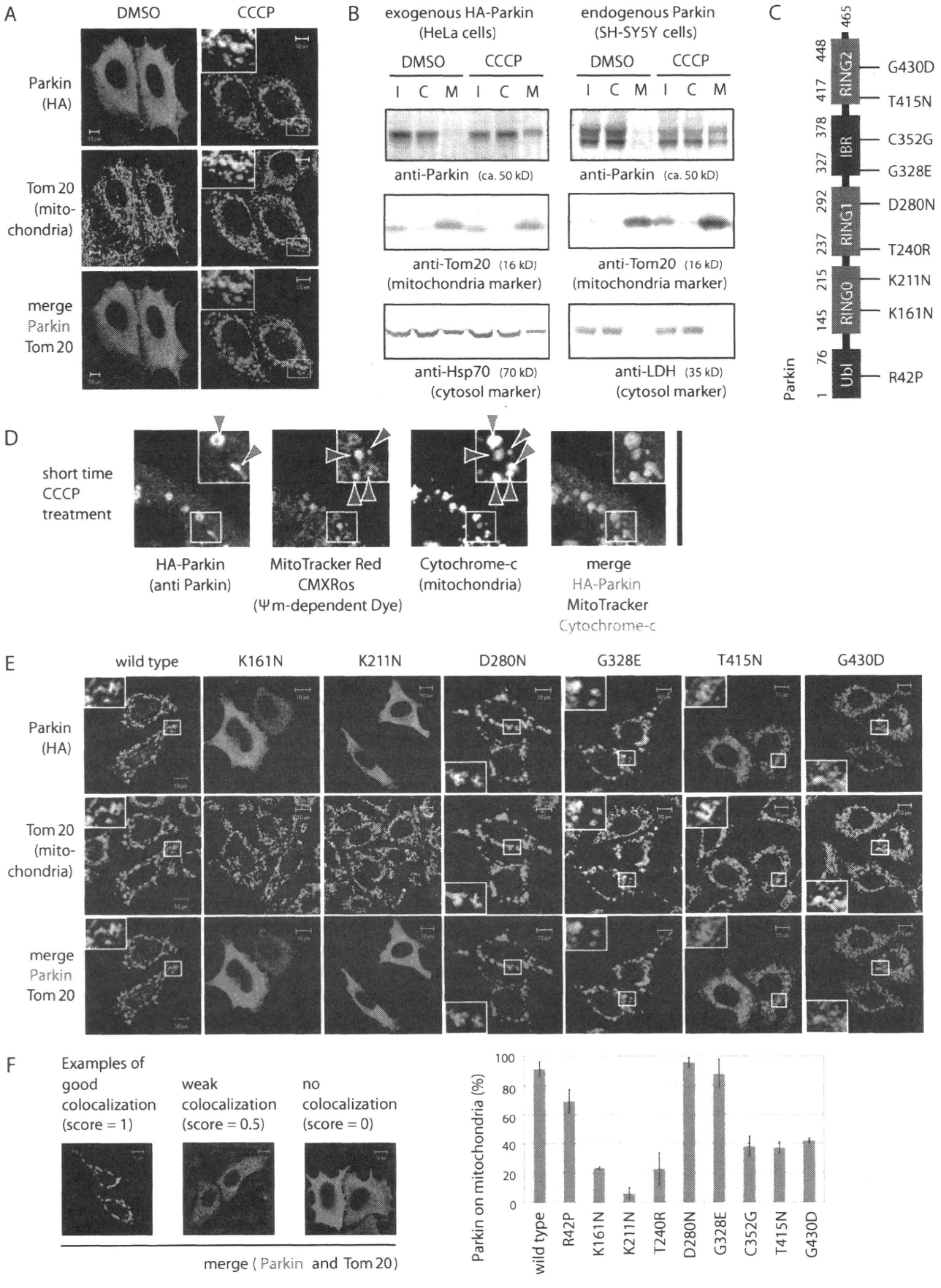
A
DMSO
CCCP
Parkin (HA)
Tom 20 (mitochondria)
merge Parkin Tom 20
B
exogenous HA-Parkin (HeLa cells)
endogenous Parkin (SH-SY5Y cells)
DMSO
CCCP
I C M I C M
anti-Parkin (ca. 50 kD)
anti-Tom20 (16 kD) (mitochondria marker)
anti-Hsp70 (70 kD) (cytosol marker)
anti-LDH (35 kD) (cytosol marker)
C
Parkin
Ubl
RING0
RING1
IBR
RING2
R42P
K161N
K211N
T240R
D280N
G328E
C352G
T415N
G430D
D
short time CCCP treatment
HA-Parkin (anti Parkin)
MitoTracker Red CMXRos (Ψm-dependent Dye)
Cytochrome-c (mitochondria)
merge HA-Parkin MitoTracker Cytochrome-c
E
wild type
K161N
K211N
D280N
G328E
T415N
G430D
Parkin (HA)
Tom 20 (mitochondria)
merge Parkin Tom 20
F
Examples of good colocalization (score = 1)
weak colocalization (score = 0.5)
no colocalization (score = 0)
merge (Parkin and Tom20)
Parkin on mitochondria (%)
100
80
60
40
20
0
wild type
R42P
K161N
K211N
T240R
D280N
G328E
C352G
T415N
G430D

regulates Parkin, and our knowledge, especially in mammals, of their relationship is limited. In this study, we describe the mechanism underlying the functional interplay between ubiquitylation catalyzed by Parkin and mitochondrial quality control regulated by PINK1.

Results and discussion

Parkin localizes to and ubiquitylates mitochondria with low membrane potential

We initially sought to study the subcellular localization and E3 activity of Parkin using HeLa cells, which reportedly lack a functional *Parkin* gene (Denison et al., 2003). In support of that study, we found that endogenous Parkin was barely detectable in HeLa cells even when PRK8, the best-characterized specific anti-Parkin antibody (Pawlyk et al., 2003), was used (Fig. S1 A). Consequently, HA-Parkin was exogenously introduced into HeLa cells. Under steady-state conditions, HA-Parkin was diffusely localized throughout the cytosol and did not overlap with mitochondria, whereas Parkin was rapidly recruited to the mitochondria when HeLa cells were treated with the mitochondrial uncoupler CCCP (carbonyl cyanide m-chlorophenylhydrazone; Fig. 1 A), as reported by Narendra et al. (2008). Next we tried to confirm the redistribution of Parkin from the cytoplasm to the mitochondria using a biochemical approach. In fractionation experiments, detection of Parkin in the mitochondria-rich fraction was faint, probably because Parkin was weakly associated with the mitochondria and thus unstable during fractionation. Inclusion of the cross-linker DSP (dithiobis[succinimidyl propionate]) significantly strengthened the signal and further confirmed redistribution of exogenous (Fig. 1 B, left) and endogenous (Fig. 1 B, right) Parkin from the cytoplasm to a mitochondria-enriched fraction. (Note that endogenous Parkin in SH-SY5Y cells is detectable as a doublet, which is consistent with a previous study [Pawlyk et al., 2003].) To more convincingly demonstrate that Parkin is selectively recruited to depolarized mitochondria, we used MitoTracker red CMXRos, which accumulates in mitochondria with an intact membrane potential. Incomplete treatment with CCCP can generate cells in which healthy and damaged mitochondria coexist. Under these conditions, signals of Parkin and MitoTracker were mutually exclusive, and Parkin selectively localized on mitochondria with lower MitoTracker red staining (Fig. 1 D), indicating that Parkin was selectively targeted to mitochondria whose membrane potential had been lost.

Subsequently, we performed immunofluorescence staining using an antiubiquitin antibody. Under normal conditions, the ubiquitin signal was spread throughout the cell. In contrast, when cells were treated with CCCP, the ubiquitin signal was concentrated in the mitochondria (Fig. 2, A and B). Mitochondrial ubiquitylation was only observed in Parkin-expressing cells (Fig. 2 A and Fig. S1 B) and disappeared when Parkin mutants deficient in E3 activity (T415N and G430D) were introduced (Fig. 2 A). Triple staining using mitochondria-targeting GFP (Mt-GFP), anti-Parkin, and anti-ubiquitin antibodies further confirmed the colocalization of Parkin, ubiquitin, and mitochondria after CCCP treatment (Fig. 2 C). Staining with single antibodies or Mt-GFP alone indicated that the aforementioned merged data were not derived from channel cross talk (Fig. S1, C and D). These results demonstrate that Parkin ubiquitylates mitochondria in response to a reduction in mitochondrial membrane potential.

Disease-relevant mutations of Parkin impair mitochondrial localization

To confirm that translocation of Parkin to depolarized mitochondria is etiologically important, we selected nine pathogenic mutations and examined their subcellular localization (Fig. 1 C). In vitro experiments have previously shown that two of the mutations (T415N and G430D) in the RING2 domain abolish E3 activity of Parkin, whereas E3 activity is unaffected by the other mutations (Hampe et al., 2006; Matsuda et al., 2006). These mutants were serially introduced into HeLa cells, followed by CCCP treatment, and their subcellular localization was examined. Parkin with the D280N or G328E mutation in RING1 or the IBR (in between RING) domain, respectively, was recruited to the mitochondria in a manner similar to wild-type Parkin (Fig. 1, E and F). In contrast, the other pathogenic mutations altered to some degree the mitochondrial localization of Parkin; in particular, the K161N, K211N, and T240R mutations, which lie in or near the RING0 domain in the linker region (Hristova et al., 2009), severely compromised the mitochondrial localization of Parkin (Fig. 1, E and F). The aforementioned results suggest that mitochondrial localization of Parkin is pathologically significant and that the RING0 domain is important for the translocation of Parkin to the damaged mitochondria.

Parkin exerts E3 activity only when the mitochondrial membrane potential decreases

As shown in Fig. 2 C and Fig. S1 B, mitochondrial ubiquitylation was dependent on Parkin translocation to the mitochondria. Thus, we tried to determine whether the subcellular localization of Parkin modulates its E3 activity. To address this issue, we monitored the E3 activity of Parkin using an

Figure 1. **Mitochondrial localization of Parkin is etiologically important.** (A) HeLa cells expressing HA-Parkin were treated with CCCP or DMSO (control) and then immunostained with the indicated antibodies. (B) HeLa cells stably expressing HA-Parkin or intact SH-SY5Y cells were treated with CCCP or DMSO and subjected to fractionation experiments. I, C, and M indicate input, cytosol-rich supernatant, and mitochondria-rich membrane pellet, respectively. (C) Schematic diagram of disease-relevant mutants of Parkin used in this study. IBR, in between RING; Ubl, ubiquitin like. (D) Polarized mitochondria stained with MitoTracker red (red arrowheads) were not labeled by Parkin. In contrast, damaged mitochondria marked by Parkin (green arrowheads) were not stained with MitoTracker red. (E) HeLa cells expressing HA-Parkin with various pathogenic mutations were treated with CCCP, followed by immunocytochemistry. (A, D, and E) Higher magnification views of the boxed areas are shown in the insets. (F) Parkin colocalization with mitochondria was analyzed in >100 cells per mutation. Example figures indicative of robust colocalization (counted as 1), weak colocalization (counted as 0.5), and no colocalization (counted as 0) are shown. Error bars represent the mean ± SD values of at least three experiments. Bars: (A, E, and F) 10 µm; (D) 30 µm.

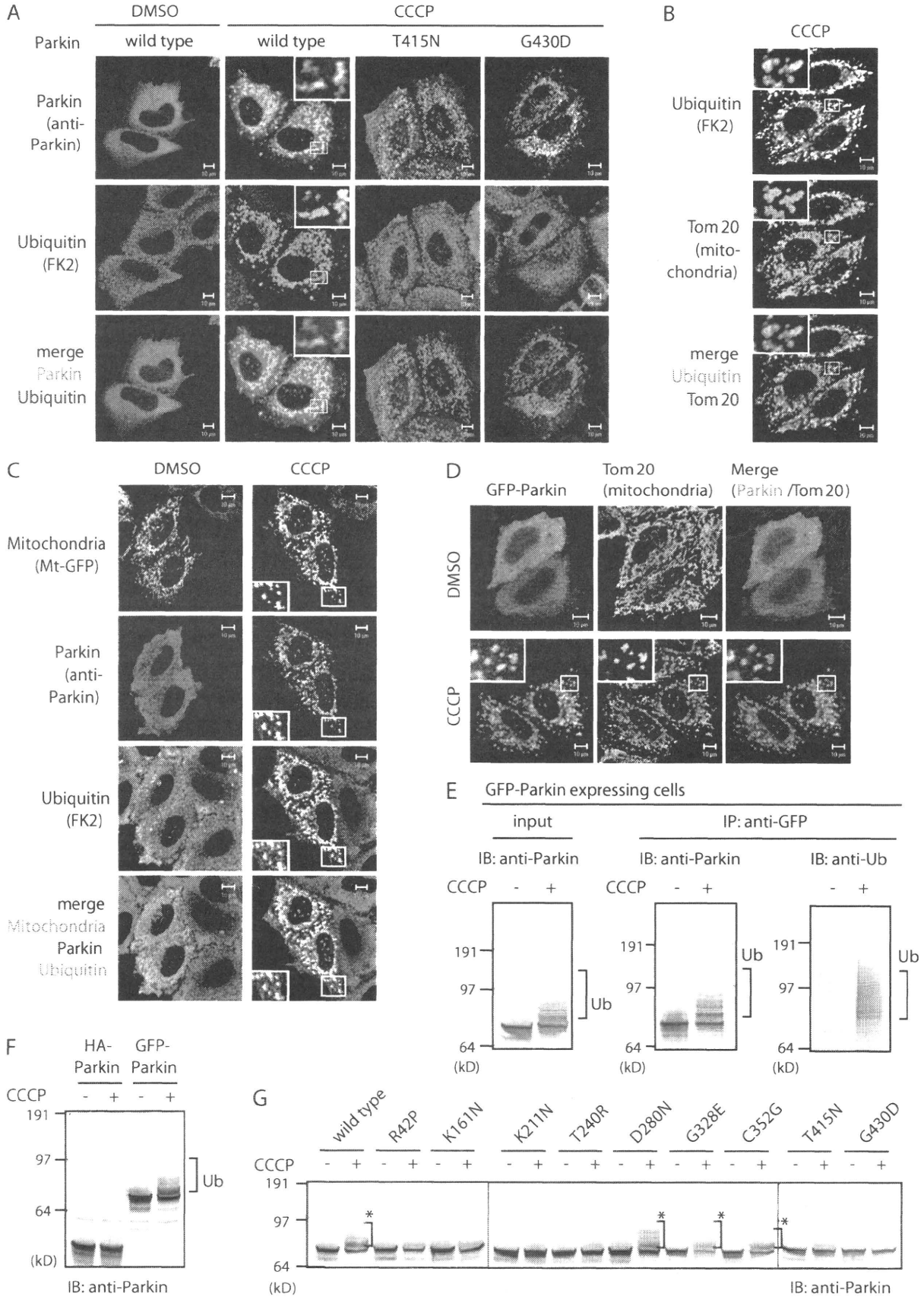

Figure 2. **Parkin exerts E3 activity only when the mitochondrial membrane potential is decreased.** (A) HeLa cells expressing wild-type Parkin or E3-inactivating mutations were treated with CCCP and then immunostained with the indicated antibodies. When E3-inactivating mutations were introduced into Parkin, the mitochondrial ubiquitylation signal disappeared. (B and C) HeLa cells expressing HA-Parkin (B) or expressing both Mt-GFP and HA-Parkin (C)

artificial substrate fused to Parkin. In vitro experiments have shown that Parkin can ubiquitylate an N-terminally fused lysine-rich protein as a pseudosubstrate (Matsuda et al., 2006). Similar ubiquitylation of pseudosubstrates even in the cytoplasm under normal conditions in vivo would be evidence that the E3 activity is constitutive; otherwise, E3 activity of Parkin is dependent on mitochondrial retrieval. A GFP tag is lysine rich and thus a good candidate for an in vivo pseudosubstrate, whereas an HA tag possesses no lysine residues and thus cannot function as a pseudosubstrate. GFP- and HA-Parkin expressed in HeLa cells treated with CCCP were both recruited to damaged mitochondria (Figs. 1 A and 2 D), but interestingly, a higher molecular mass population of only GFP-Parkin was observed (Fig. 2 F). Immunoprecipitation experiments demonstrated that GFP-Parkin was indeed ubiquitylated (Fig. 2 E). This was not based on autoubiquitylation of Parkin itself because mitochondria-associated HA-Parkin did not undergo ubiquitylation after CCCP treatment (Fig. 2 F and not depicted). Moreover, ubiquitylation of GFP-Parkin was absent in the T415N and G430D mutants, which lack E3 activities, suggesting that ubiquitylation of GFP-Parkin is not derived from other E3s (Fig. 2 G). The K161N and K211N mutants that impaired mitochondrial localization also inhibited ubiquitylation of GFP-Parkin (Fig. 2 G). Collectively, the aforementioned results indicate that Parkin ubiquitylates fused GFP only when it is retrieved to the mitochondria, suggesting that the latent E3 activity of Parkin is dependent on decreased mitochondrial membrane potential.

PINK1 localization is stabilized by damaged mitochondria

Recessive mutations in the human *PINK1* gene are also the cause of autosomal recessive early-onset PD (Valente et al., 2004). We next examined whether the subcellular localization of PINK1 was affected by mitochondrial membrane potential. As reported previously (Valente et al., 2004; Beilina et al., 2005; Takatori et al., 2008), N-terminal Myc– or N-terminal Flag–tagged PINK1 clearly localized to the mitochondria, whereas C-terminal Flag– or C-terminal V5–tagged PINK1 mainly localized to the cytoplasm (Fig. 3 A and not depicted). Exogenous nontagged PINK1 also localized to the cytoplasm under steady-state conditions (Fig. 3 B), suggesting that mitochondrial localization of PINK1 is an artifact of the N-terminal epitope. More importantly, similar to Parkin, untagged PINK1 and C-terminal Flag– or C-terminal V5–tagged PINK1 localized to the mitochondria after CCCP treatment (Fig. 3, A and B; and not depicted). These results suggest that the subcellular localization of PINK1 is also regulated by the mitochondrial membrane potential.

We next sought to determine the subcellular localization of endogenous PINK1. Immunocytochemical experiments showed, as reported previously (Zhou et al., 2008), that the endogenous PINK1 signal was barely detectable in HeLa cells under steady-state conditions. However, a decrease in mitochondrial membrane potential resulted in a mitochondria-associated PINK1 signal (Fig. 3, C and D). We found that CCCP treatment promoted the gradual accumulation of endogenous PINK1 in immunoblots as well (Fig. 3 E) and the presence of endogenous PINK1 in a mitochondria-enriched fraction (Fig. 3 F). More importantly, when CCCP was washed out, the accumulated endogenous PINK1 rapidly disappeared (within 30 min) both in the presence and absence of cycloheximide (Fig. 3 G and not depicted). Moreover, the N-terminal 34 aa of PINK1 sufficiently recruited GFP to the mitochondria even in the absence of CCCP (Fig. 3 H). These results support the hypothesis in which PINK1 is constantly transported to the mitochondria but is rapidly degraded in a membrane potential–dependent manner. We speculate that PINK1 is stabilized by a decrease in mitochondrial membrane potential and, as a result, accumulates in depolarized mitochondria.

PINK1 normally exists as either a long (~60 kD) or a short (~50 kD) protein. Because the canonical mitochondria-targeting signal (matrix-targeting signal) is cleaved after import into the mitochondria, the long form has been designated as the precursor and the short form as the mature PINK1 (Beilina et al., 2005; Silvestri et al., 2005). The short (processed) form of PINK1 was clearly detected when untagged PINK1 was overexpressed (Fig. 3 E, sixth lane); however, this form of endogenous PINK1 was rarely detectable after CCCP treatment (Fig. 3 E, the first through the fifth lanes). Our subcellular localization study of endogenous PINK1 after CCCP treatment showed that the long form was recovered in the mitochondrial fraction (Fig. 3 F), suggesting that it is not the preimport precursor form. Moreover, by monitoring the degradation process of PINK1 after recovery of membrane potential, we realized that the short form of PINK1 transiently appeared soon after CCCP was washed out and then later disappeared (Fig. 3 G), suggesting that the processed form of PINK1 is an intermediate in membrane potential–dependent degradation. In conclusion, these results imply that PINK1 cleavage dose not reflect a canonical maturation process accompanying mitochondrial import as initially thought.

PINK1 retrieves Parkin from the cytoplasm to the mitochondria

Because previous studies revealed that PINK1 functions upstream of Parkin (Clark et al., 2006; Park et al., 2006; Yang et al., 2006; Exner et al., 2007), we next examined the potential role of PINK1 in the mitochondrial recruitment of Parkin. To obtain clear-cut conclusions, we set up our experimental system using mouse embryonic fibroblasts (MEFs) derived from control

were treated with CCCP or DMSO (control) and then immunostained with the indicated antibodies. (D) Localization of GFP-Parkin to the mitochondria after CCCP treatment. (A–D) Higher magnification views of the boxed areas are shown in the insets. (E) HeLa cell lysates expressing GFP-Parkin were immunoprecipitated by anti-GFP antibody, followed by immunoblotting with the indicated antibodies. (F) Straight immunoblotting of HA- and GFP-Parkin in the absence or presence of CCCP. Note the slower migrating ladders derived from ubiquitylation (Ub) in only the GFP-Parkin with CCCP lane. (G) GFP-Parkin–expressing HeLa cells with various pathogenic mutations (Fig. 1 C) were treated with CCCP and subjected to immunoblotting. Asterisks show ubiquitylation of GFP-Parkin. Vertical black lines indicate that intervening lanes have been spliced out. IB, immunoblot; IP, immunoprecipitation. Bars, 10 µm.

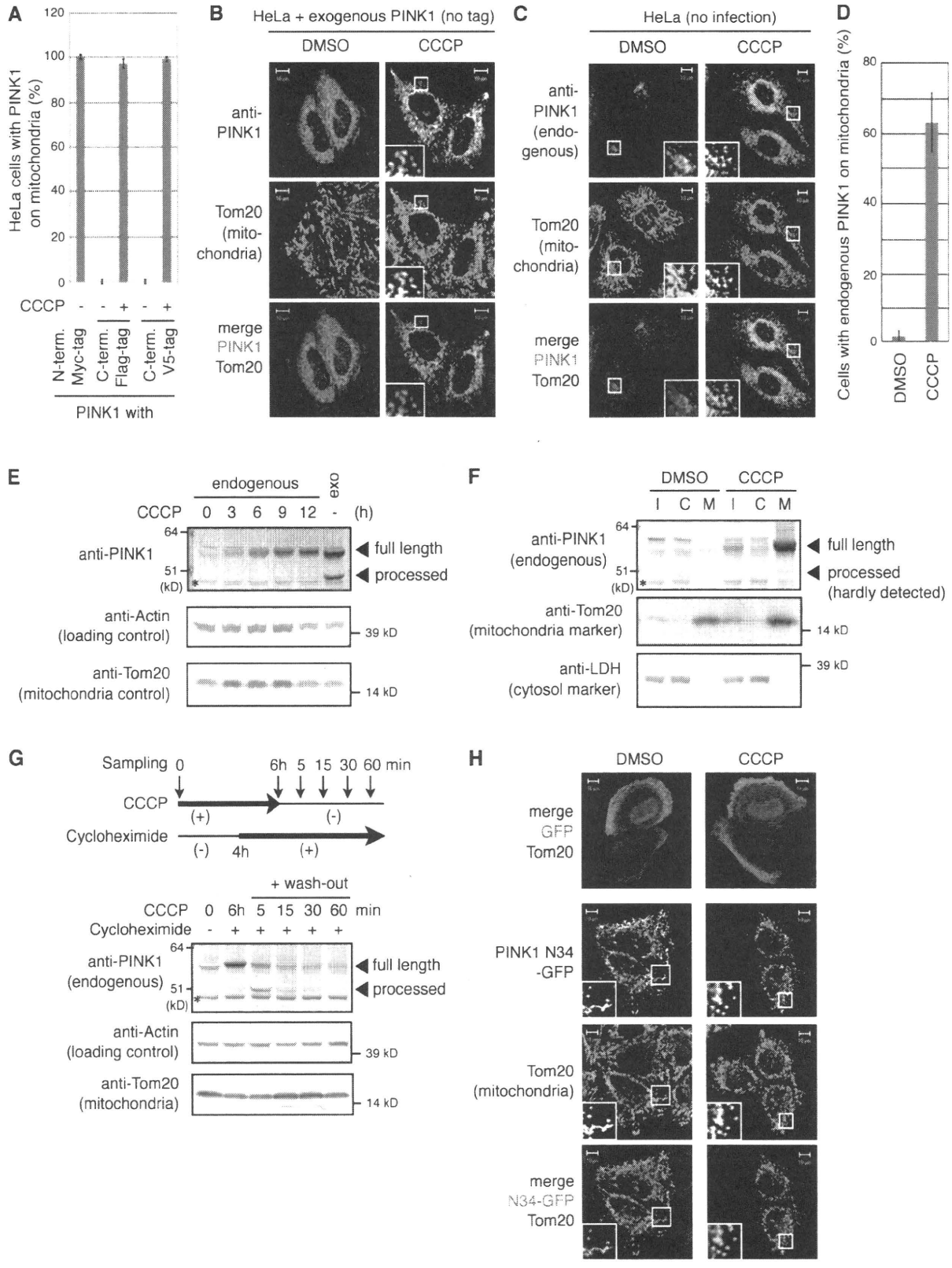

Figure 3. **PINK1 is constitutively degraded in a mitochondrial membrane potential–dependent manner and localizes to depolarized mitochondria.** (A) The number of HeLa cells with N-terminal– or C-terminal–tagged PINK1 localized to the mitochondria was counted in >100 cells. (B and C) Exogenous non-tagged PINK1 (B) or endogenous PINK1 (C) in HeLa cells was immunostained with the indicated antibodies. (D) The number of HeLa cells with endogenous PINK1 localized to the mitochondria was counted as in A. (A and D) Error bars represent the mean ± SD values of least three experiments. (E) Endogenous PINK1 gradually accumulated after CCCP treatment. The first through the fifth lanes show endogenous PINK1, and the sixth lane shows overexpressed untagged PINK1. Note that the asterisk indicates a cross-reacting band because it was not affected by overproduction of untagged PINK1. (F) Subcellular fractionation of endogenous PINK1. Intact SH-SY5Y cells were treated with CCCP or DMSO and subjected to fractionation experiments (same sample as

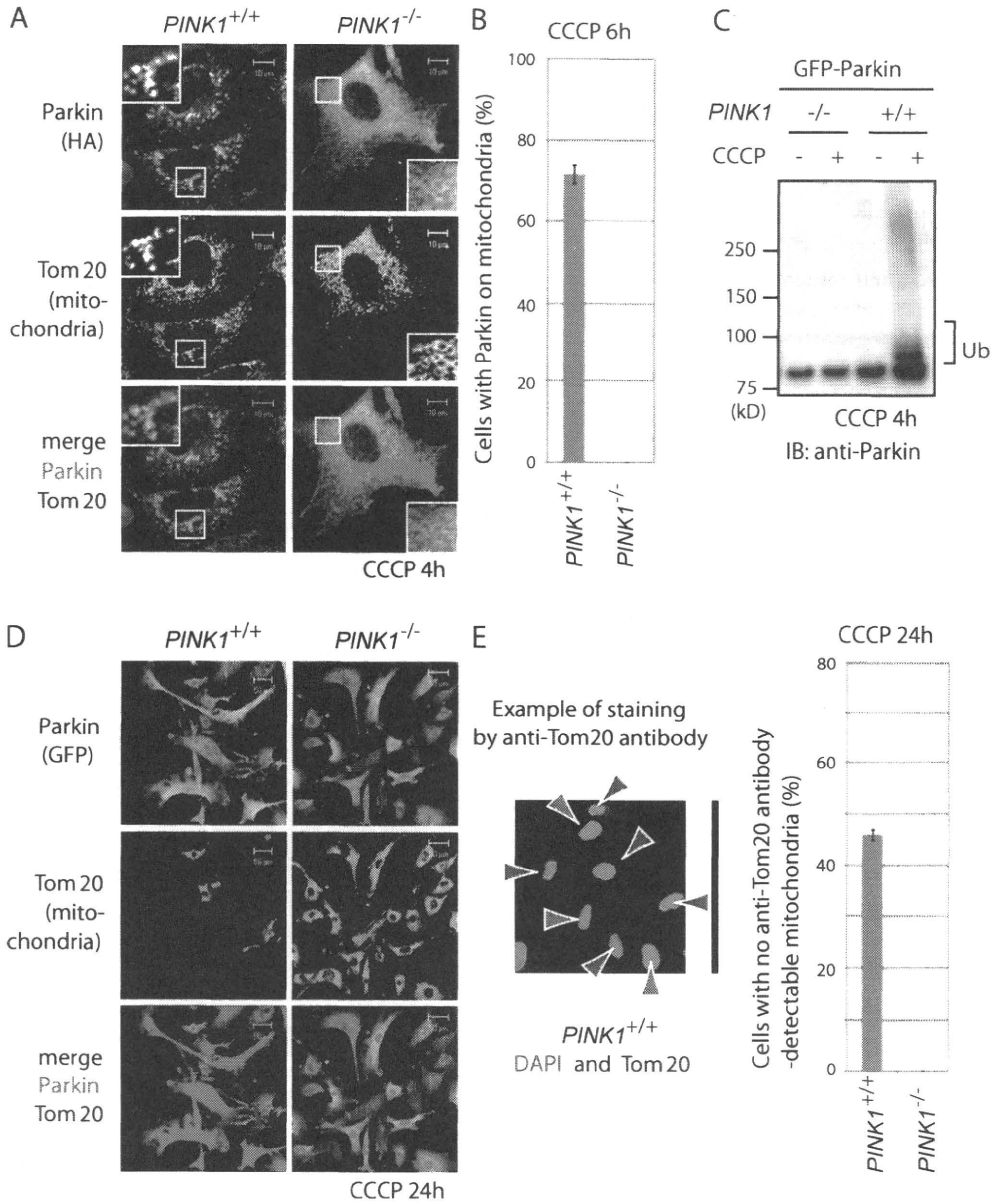

Figure 4. **PINK1 recruits cytoplasmic Parkin to damaged mitochondria.** (A) *PINK1* knockout (*PINK1*$^{-/-}$) or control (*PINK1*$^{+/+}$) MEFs were transfected with HA-Parkin, treated with CCCP, and subjected to immunocytochemistry with the indicated antibodies. Higher magnification views of the boxed areas are shown in the insets. (B) The number of MEFs with Parkin localized to the mitochondria was counted as in Fig. 3 A. (C and D) Neither activation of Parkin nor mitochondrial degradation was observed in *PINK1*$^{-/-}$ MEFs. MEFs stably expressing GFP-Parkin were treated with CCCP for 4 h and subjected to immunoblotting (C) or for 24 h, followed by immunocytochemistry (D). IB, immunoblot; Ub, ubiquitylation. (E) The number of MEFs without anti-Tom20 antibody–detectable mitochondria was counted as in Fig. 3 A. In the example figure (left), blue arrowheads indicate cells without anti-Tom20 antibody–detectable mitochondria, and red arrowheads indicate cells harboring anti-Tom20 antibody–detectable mitochondria. (B and E) Error bars represent the mean ± SD values of least three experiments. Bars: (A) 10 µm; (D) 50 µm; (E) 150 µm.

(*PINK1*$^{+/+}$) or *PINK1* knockout (*PINK1*$^{-/-}$) mouse (Gautier et al., 2008). Endogenous Parkin is undetectable in MEFs (Fig. S1 A); consequently, HA- or GFP-Parkin was introduced into these cells by retroviral transfection (Kitamura et al., 2003). In control MEFs (*PINK1*$^{+/+}$), Parkin was selectively recruited to the mitochondria after CCCP treatment (Fig. 4 A) and subsequently resulted in the disappearance of the mitochondria (Fig. 4, D and E). This mitochondrial clearance was considerably impeded by *Atg7* (essential gene for autophagy) knockout (Fig. S2; Komatsu et al., 2005), suggesting that Parkin degrades mitochondria by selective autophagy as reported previously (Narendra et al., 2008). In sharp contrast, Parkin was not

Fig. 1 B). I, C, and M indicate input, cytosol-rich supernatant, and the mitochondria-rich membrane pellet, respectively. (G) HeLa cells were treated with CCCP and cycloheximide as depicted, followed by immunoblotting with the indicated antibodies. LDH, lactate dehydrogenase. (F and G) Asterisks indicate a cross-reacting band. (H) N-terminal 34 aa of PINK1 recruited GFP to the mitochondria both in the absence and presence of CCCP. The top panel shows control HeLa cells expressing only GFP. (B, C, and H) Higher magnification views of the boxed areas are shown in the insets. Bars, 10 µm.

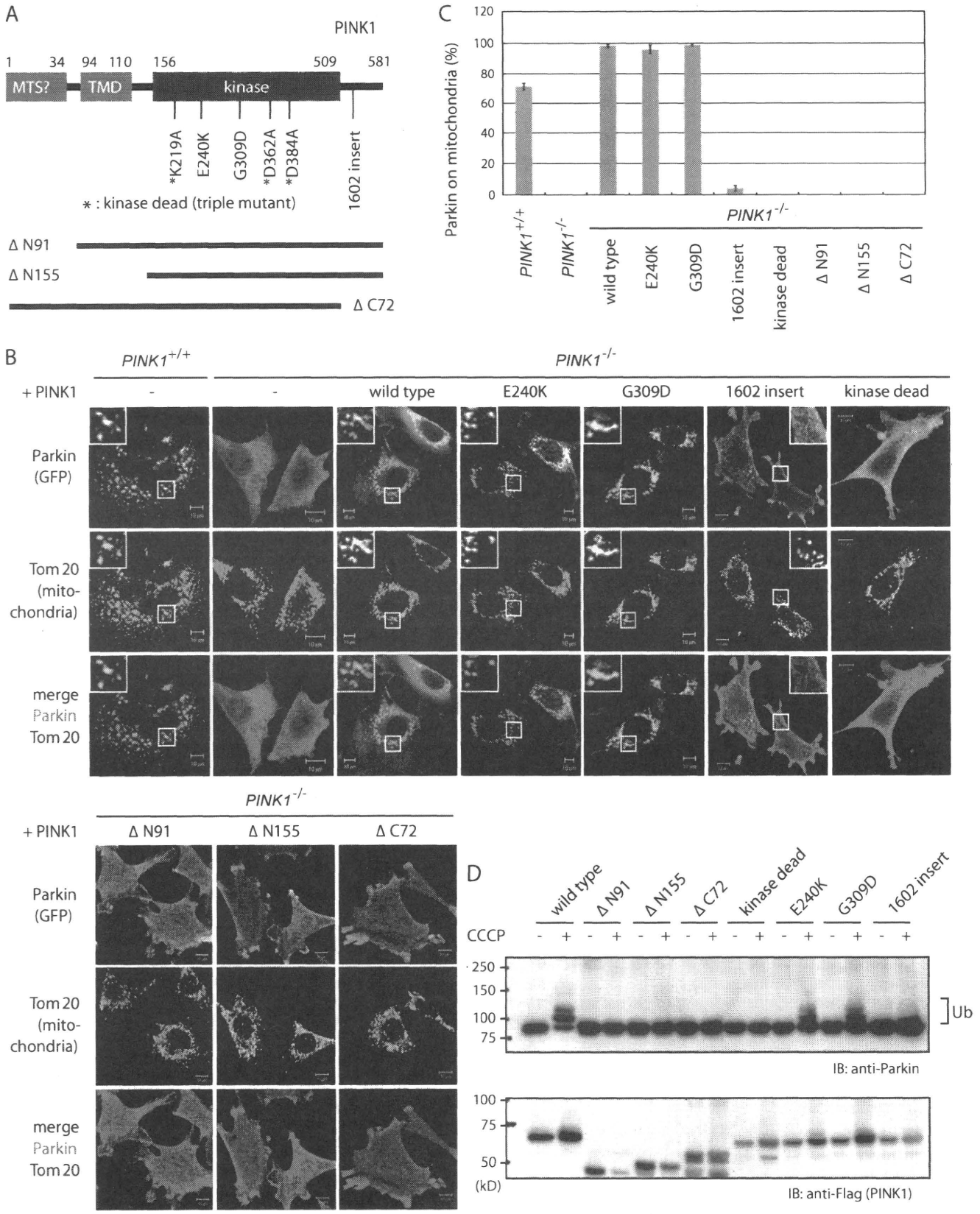

Figure 5. **Kinase activity and mitochondrial targeting of PINK1 is imperative for mitochondrial localization of Parkin.** (A) Schematic depiction of pathogenic and deletion mutants of PINK1 used in this study. MTS, mitochondria-targeting sequence; TMD, transmembrane domain. (B) Subcellular localization of Parkin in *PINK1*$^{-/-}$ cells complemented by various pathogenic and deletion mutants of PINK1-Flag. Cells were treated with CCCP. Higher magnification views of the boxed areas are shown in the insets. (C) The number of cells with Parkin-positive mitochondria was counted as in Fig. 3 A. Error bars represent the mean ± SD values of least three experiments. (D) *PINK1*$^{-/-}$ MEFs complemented by various PINK1 mutants were treated with CCCP and subjected to immunoblotting using anti-Parkin or anti-Flag (tag of PINK1) antibodies. IB, immunoblot; Ub, ubiquitylation. Bars, 10 μm.

translocated to the mitochondria in *PINK1* knockout (*PINK1*$^{-/-}$) MEFs after CCCP treatment (Fig. 4, A and B). Subsequent activation of Parkin and mitochondrial degradation were also completely impeded (Fig. 4, C–E). To exclude the possible role of retroviral integration of Parkin in the aforementioned phenotype, we checked whether reintroduction of PINK1 rescued this phenotype. Untagged or C-terminal Flag–tagged PINK1 complemented the mislocalization of Parkin in *PINK1*$^{-/-}$ MEFs (Fig. 5, B and C; and not depicted), confirming that the aforementioned defects were caused by the loss of PINK1.

To examine whether pathogenic mutations of PINK1 affect its mitochondrial localization, we expressed PINK1 mutants harboring the missense mutations E240K and G309D, or a CAA nucleotide insertion behind C1602 (referred to hereafter as 1602-insert) in *PINK1*$^{-/-}$ MEFs. Similar to wild-type PINK1, these PINK1 mutants colocalized with mitochondria after CCCP treatment (Fig. S3). Next, GFP-Parkin was introduced into these cells to examine whether pathogenic mutations of PINK1 affect the mitochondrial localization and activation of Parkin. The E240K and G309D mutants restored the mitochondrial localization and activation of Parkin as well as wild-type PINK1, whereas recruitment of Parkin to the mitochondria by the 1602-insert mutant was abolished (Fig. 5, B–D), suggesting that the pathology of this PINK1 mutation is mislocalization and consequent inactivation of Parkin.

Mitochondrial localization and kinase activity of PINK1 are essential for translocation of Parkin to damaged mitochondria

Finally, we investigated the role of various PINK1 domains (Fig. 5 A) in the mitochondrial recruitment of Parkin. PINK1 is composed of an atypical N-terminal mitochondrial localization signal and transmembrane domain, a kinase domain in the middle, and a conserved C-terminal domain (Zhou et al., 2008). Deletion of the N-terminal 91 aa abolished the mitochondrial localization of PINK1 (Zhou et al., 2008). We also confirmed that the ΔN91 and ΔN155 mutants did not target to the mitochondria even after CCCP treatment (Fig. S3). We also generated a mutant containing the triple K219A, D362A, and D384A mutations that abolish kinase activity (Beilina et al., 2005) and a C-terminal domain deletion mutant associated with PINK1 dysfunction (Sim et al., 2006; Yang et al., 2006). The kinase-dead and ΔC72 mutants of PINK1 colocalized with damaged mitochondria similar to wild type (Fig. S3). When introduced into *PINK1*$^{-/-}$ cells harboring GFP-Parkin, the mutants were unable to complement the mislocalization and inactivation of Parkin (Fig. 5, B–D), even though the mutant PINK1 proteins were expressed (Fig. 5 D and Fig. S3). These results indicate that the kinase activity and mitochondrial targeting of PINK1 are essential for the mitochondrial recruitment of Parkin.

Conclusion

In summary, we have shown that (a) PINK1 is a Parkin-recruitment factor that recruits Parkin from the cytoplasm to damaged mitochondria in a membrane potential–dependent manner for mitochondrial degradation, (b) endogenous PINK1 is constitutively degraded at the mitochondria, but its localization is specifically linked to a decrease in membrane potential, (c) under steady-state conditions, the E3 activity of Parkin is repressed in the cytoplasm but is liberated by PINK1-dependent mitochondrial localization, and (d) the aforementioned phenomena are presumably etiologically important in part because they were impeded for the most part by disease-linked mutations of PINK1 or Parkin. We believe that these results provide solid insight into the molecular mechanisms of PD pathogenesis not only for familial forms caused by *Parkin* and *PINK1* mutations but also major sporadic forms of PD.

Materials and methods

Cell culture and transfection

MEFs derived from embryonic day 12.5 embryos of PINK1 knockout mice (provided by J. Shen, Harvard Medical School, Boston, MA) were mechanically dispersed by repeated passage through a P1000 pipette tip and plated with MEF media containing DME, 10% FCS, β-mercaptoethanol (Sigma-Aldrich), 1× nonessential amino acids, and 1 mM L-glutamine. Various stable transformants of MEFs were established by infecting MEFs with recombinant retroviruses. HA-Parkin, GFP-Parkin, PINK1 (provided by Y. Nakamura, T. Iwatsubo, and S. Takatori, University of Tokyo, Bunkyo-ku, Tokyo, Japan), or various PINK1 mutants were cloned into a pMXs-puro vector. Retrovirus packaging cells, PLAT-E (provided by T. Kitamura, University of Tokyo; Kitamura et al., 2003), were transfected with the aforementioned vectors and were cultured at 37°C for 24 h. After changing the medium, cells were further incubated at 37°C for 24 h, and the viral supernatant was collected and used for infection. MEFs were plated on 35-mm dishes at 24 h before infection, and the medium was replaced with the aforementioned undiluted viral supernatant with 8 μg/ml polybrene (Sigma-Aldrich). 2 d later, transformants were selected by the medium containing 10 μg/ml puromycin.

Cell fractionation and immunoprecipitation

To depolarize the mitochondria, HeLa and SH-SY5Y cells were treated with 10 μM CCCP, and MEFs were treated with 30 μM CCCP. For fractionation experiments, HeLa and SH-SY5Y cells were treated with CCCP for 1–5 h and subsequently treated with 1 mM DSP (Thermo Fisher Scientific) in PBS for 1 h on ice, inactivated by 10 mM glycine in PBS three times, and suspended in chappell-perry buffer (0.15 M KCl, 20 mM Hepes-NaOH, pH 8.1, 5 mM $MgCl_2$, and protease and phosphatase inhibitor [Roche]). Cells were disrupted by five passages through a 25-gauge needle (with 1-ml syringe), debris was removed by centrifugation at 1,000 *g* for 7 min, and the supernatant was subjected to 10,000 *g* for 10 min to separate the mitochondria-rich fraction from the cytosol-rich fraction. Immunoblotting and immunoprecipitation were performed by conventional methods. To detect the ubiquitylation of GFP-Parkin, the cell lysate of HeLa cells (10 μM CCCP for 1 h) or MEFs (30 μM CCCP for 3 h) was collected in the presence of 10 mM N-ethylmaleimide to protect ubiquitylated Parkin from deubiquitylation enzymes. To monitor the degradation of endogenous PINK1, HeLa cells were treated with 10 μM CCCP and 50 μg/ml cycloheximide as depicted in Fig. 3 G and were subjected to immunoblotting.

Immunocytochemistry

To depolarize the mitochondria, HeLa cells (provided by A. Tanaka and R. Youle, National Institutes of Health, Bethesda, MD) were treated with 10 μM CCCP for 1 h (exogenous Parkin and PINK1) or 5 h (endogenous PINK1), and MEFs were treated with 30 μM CCCP for 3–4 h (Figs. 4 A and 5 B; and Fig. S3 B) or 24 h (Fig. 4 D and Fig. S2 A). For immunofluorescence experiments, cells were fixed with 4% paraformaldehyde, permeabilized with 50 μg/ml digitonin, and stained with primary antibodies described in the next section and with the following secondary antibodies: mouse and/or rabbit Alexa Fluor 488, 568, and 647 (Invitrogen). N-terminal 34 aa of PINK1 were fused to GFP to stain mitochondria in the triple staining experiments. To monitor the mitochondrial membrane potential, MEFs were treated with 50 nM MitoTracker red CMXRos (Invitrogen) for 15 min, washed three times, and incubated for an additional 10 min before fixation, as reported previously (Narendra et al., 2008). Cells were imaged using a laser-scanning microscope (LSM510 META; Carl Zeiss, Inc.) with a Plan-Apochromat 63× NA 1.4 oil differential interference contrast objective lens. Image contrast and brightness were adjusted in Photoshop (Adobe).

Antibodies

Antibodies used in this study are as follows: antiactin (AC-40; Sigma-Aldrich), anti–cytochrome c (6H2.B4; BD), anti-Flag (M2; Sigma-Aldrich), anti-GFP (3E6 [Wako Chemicals USA, Inc.]; or A6455 [Invitrogen]), anti-HA (12CA5; Roche), anti-Hsp70 (MBL), anti–lactate dehydrogenase (Abcam), anti-Parkin (#2132 [Cell Signaling Technology] for immunocytochemistry; or PRK8 [Sigma-Aldrich] for immunoblotting), anti-PINK1 (Novus), anti-Tom20 (FL-145 and F-10; Santa Cruz Biotechnology, Inc.), antiubiquitin (P4D1 [Santa Cruz Biotechnology, Inc.]; or FK2 [MBL]), and anti-V5 (Invitrogen).

Online supplemental material

Fig. S1 shows various control experiments for immunoblotting and immunocytochemistry. Fig. S2 shows that Parkin promoted degradation of depolarized mitochondria via autophagy. Fig. S3 shows the subcellular localization of pathogenic and deletion mutants of PINK1 after CCCP treatment. Online supplemental material is available at http://www.jcb.org/cgi/content/full/jcb.200910140/DC1.

We thank Dr. T. Kitamura for providing the PLAT-E cells, Drs. A. Tanaka and R. Youle for NIH HeLa cells, Dr. J. Shen for *PINK1* knockout MEFs, and Drs. Y. Nakamura, T. Iwatsubo, and S. Takatori for plasmids.

This work was supported by Grants-in-Aid for Young Scientist (B) (to N. Matsuda, K. Shiba, and S. Saiki) and by Specially Promoted Research (to K. Tanaka) from the Ministry of Education, Culture, Sports, Science and Technology of Japan and Heath and Labor Science Research grants (to N. Hattori and K. Tanaka).

Note added in review. While our manuscript was under review, Geisler et al. (2010), Narendra et al. (2010), and Vives-Bauza et al. (2010) independently published results that are consistent with those described herein.

Submitted: 26 October 2009
Accepted: 22 March 2010

References

Beilina, A., M. Van Der Brug, R. Ahmad, S. Kesavapany, D.W. Miller, G.A. Petsko, and M.R. Cookson. 2005. Mutations in PTEN-induced putative kinase 1 associated with recessive parkinsonism have differential effects on protein stability. *Proc. Natl. Acad. Sci. USA.* 102:5703–5708. doi:10.1073/pnas.0500617102

Clark, I.E., M.W. Dodson, C. Jiang, J.H. Cao, J.R. Huh, J.H. Seol, S.J. Yoo, B.A. Hay, and M. Guo. 2006. *Drosophila* pink1 is required for mitochondrial function and interacts genetically with parkin. *Nature.* 441: 1162–1166. doi:10.1038/nature04779

Denison, S.R., F. Wang, N.A. Becker, B. Schüle, N. Kock, L.A. Phillips, C. Klein, and D.I. Smith. 2003. Alterations in the common fragile site gene Parkin in ovarian and other cancers. *Oncogene.* 22:8370–8378. doi:10.1038/sj.onc.1207072

Dodson, M.W., and M. Guo. 2007. Pink1, Parkin, DJ-1 and mitochondrial dysfunction in Parkinson's disease. *Curr. Opin. Neurobiol.* 17:331–337. doi:10.1016/j.conb.2007.04.010

Exner, N., B. Treske, D. Paquet, K. Holmström, C. Schiesling, S. Gispert, I. Carballo-Carbajal, D. Berg, H.H. Hoepken, T. Gasser, et al. 2007. Loss-of-function of human PINK1 results in mitochondrial pathology and can be rescued by parkin. *J. Neurosci.* 27:12413–12418. doi:10.1523/JNEUROSCI.0719-07.2007

Gautier, C.A., T. Kitada, and J. Shen. 2008. Loss of PINK1 causes mitochondrial functional defects and increased sensitivity to oxidative stress. *Proc. Natl. Acad. Sci. USA.* 105:11364–11369. doi:10.1073/pnas.0802076105

Geisler, S., K.M. Holmström, D. Skujat, F.C. Fiesel, O.C. Rothfuss, P.J. Kahle, and W. Springer. 2010. PINK1/Parkin-mediated mitophagy is dependent on VDAC1 and p62/SQSTM1. *Nat. Cell Biol.* 12:119–131. doi:10.1038/ncb2012

Hampe, C., H. Ardila-Osorio, M. Fournier, A. Brice, and O. Corti. 2006. Biochemical analysis of Parkinson's disease-causing variants of Parkin, an E3 ubiquitin-protein ligase with monoubiquitylation capacity. *Hum. Mol. Genet.* 15:2059–2075. doi:10.1093/hmg/ddl131

Hardy, J., H. Cai, M.R. Cookson, K. Gwinn-Hardy, and A. Singleton. 2006. Genetics of Parkinson's disease and parkinsonism. *Ann. Neurol.* 60:389–398. doi:10.1002/ana.21022

Hristova, V.A., S.A. Beasley, R.J. Rylett, and G.S. Shaw. 2009. Identification of a novel Zn2+-binding domain in the autosomal recessive juvenile Parkinson-related E3 ligase parkin. *J. Biol. Chem.* 284:14978–14986. doi:10.1074/jbc.M808700200

Imai, Y., M. Soda, and R. Takahashi. 2000. Parkin suppresses unfolded protein stress-induced cell death through its E3 ubiquitin-protein ligase activity. *J. Biol. Chem.* 275:35661–35664. doi:10.1074/jbc.C000447200

Kitada, T., S. Asakawa, N. Hattori, H. Matsumine, Y. Yamamura, S. Minoshima, M. Yokochi, Y. Mizuno, and N. Shimizu. 1998. Mutations in the parkin gene cause autosomal recessive juvenile parkinsonism. *Nature.* 392:605–608. doi:10.1038/33416

Kitamura, T., Y. Koshino, F. Shibata, T. Oki, H. Nakajima, T. Nosaka, and H. Kumagai. 2003. Retrovirus-mediated gene transfer and expression cloning: powerful tools in functional genomics. *Exp. Hematol.* 31:1007–1014.

Komatsu, M., S. Waguri, T. Ueno, J. Iwata, S. Murata, I. Tanida, J. Ezaki, N. Mizushima, Y. Ohsumi, Y. Uchiyama, et al. 2005. Impairment of starvation-induced and constitutive autophagy in Atg7-deficient mice. *J. Cell Biol.* 169:425–434. doi:10.1083/jcb.200412022

Lim, K.L. 2007. Ubiquitin-proteasome system dysfunction in Parkinson's disease: current evidence and controversies. *Expert Rev. Proteomics.* 4:769–781. doi:10.1586/14789450.4.6.769

Matsuda, N., and K. Tanaka. 2010. Does impairment of the ubiquitin-proteasome system or the autophagy-lysosome pathway predispose individuals to neurodegenerative disorders such as Parkinson's disease? *J. Alzheimers Dis.* 19:1–9.

Matsuda, N., T. Kitami, T. Suzuki, Y. Mizuno, N. Hattori, and K. Tanaka. 2006. Diverse effects of pathogenic mutations of Parkin that catalyze multiple monoubiquitylation in vitro. *J. Biol. Chem.* 281:3204–3209. doi:10.1074/jbc.M510393200

Moore, D.J., A.B. West, V.L. Dawson, and T.M. Dawson. 2005. Molecular pathophysiology of Parkinson's disease. *Annu. Rev. Neurosci.* 28:57–87. doi:10.1146/annurev.neuro.28.061604.135718

Narendra, D., A. Tanaka, D.F. Suen, and R.J. Youle. 2008. Parkin is recruited selectively to impaired mitochondria and promotes their autophagy. *J. Cell Biol.* 183:795–803. doi:10.1083/jcb.200809125

Narendra, D.P., S.M. Jin, A. Tanaka, D.F. Suen, C.A. Gautier, J. Shen, M.R. Cookson, and R.J. Youle. 2010. PINK1 is selectively stabilized on impaired mitochondria to activate Parkin. *PLoS Biol.* 8:e1000298. doi:10.1371/journal.pbio.1000298

Park, J., S.B. Lee, S. Lee, Y. Kim, S. Song, S. Kim, E. Bae, J. Kim, M. Shong, J.M. Kim, and J. Chung. 2006. Mitochondrial dysfunction in *Drosophila* PINK1 mutants is complemented by parkin. *Nature.* 441:1157–1161. doi:10.1038/nature04788

Pawlyk, A.C., B.I. Giasson, D.M. Sampathu, F.A. Perez, K.L. Lim, V.L. Dawson, T.M. Dawson, R.D. Palmiter, J.Q. Trojanowski, and V.M. Lee. 2003. Novel monoclonal antibodies demonstrate biochemical variation of brain parkin with age. *J. Biol. Chem.* 278:48120–48128. doi:10.1074/jbc.M306889200

Schapira, A.H. 2008. Mitochondria in the aetiology and pathogenesis of Parkinson's disease. *Lancet Neurol.* 7:97–109. doi:10.1016/S1474-4422(07)70327-7

Shimura, H., N. Hattori, S. Kubo, Y. Mizuno, S. Asakawa, S. Minoshima, N. Shimizu, K. Iwai, T. Chiba, K. Tanaka, and T. Suzuki. 2000. Familial Parkinson disease gene product, parkin, is a ubiquitin-protein ligase. *Nat. Genet.* 25:302–305. doi:10.1038/77060

Silvestri, L., V. Caputo, E. Bellacchio, L. Atorino, B. Dallapiccola, E.M. Valente, and G. Casari. 2005. Mitochondrial import and enzymatic activity of PINK1 mutants associated to recessive parkinsonism. *Hum. Mol. Genet.* 14:3477–3492. doi:10.1093/hmg/ddi377

Sim, C.H., D.S. Lio, S.S. Mok, C.L. Masters, A.F. Hill, J.G. Culvenor, and H.C. Cheng. 2006. C-terminal truncation and Parkinson's disease-associated mutations down-regulate the protein serine/threonine kinase activity of PTEN-induced kinase-1. *Hum. Mol. Genet.* 15:3251–3262. doi:10.1093/hmg/ddl398

Takatori, S., G. Ito, and T. Iwatsubo. 2008. Cytoplasmic localization and proteasomal degradation of N-terminally cleaved form of PINK1. *Neurosci. Lett.* 430:13–17. doi:10.1016/j.neulet.2007.10.019

Valente, E.M., P.M. Abou-Sleiman, V. Caputo, M.M. Muqit, K. Harvey, S. Gispert, Z. Ali, D. Del Turco, A.R. Bentivoglio, D.G. Healy, et al. 2004. Hereditary early-onset Parkinson's disease caused by mutations in PINK1. *Science.* 304:1158–1160. doi:10.1126/science.1096284

Vives-Bauza, C., C. Zhou, Y. Huang, M. Cui, R.L. de Vries, J. Kim, J. May, M.A. Tocilescu, W. Liu, H.S. Ko, et al. 2010. PINK1-dependent recruitment of Parkin to mitochondria in mitophagy. *Proc. Natl. Acad. Sci. USA.* 107:378–383. doi:10.1073/pnas.0911187107

Yang, Y., S. Gehrke, Y. Imai, Z. Huang, Y. Ouyang, J.W. Wang, L. Yang, M.F. Beal, H. Vogel, and B. Lu. 2006. Mitochondrial pathology and muscle and dopaminergic neuron degeneration caused by inactivation of *Drosophila* Pink1 is rescued by Parkin. *Proc. Natl. Acad. Sci. USA.* 103:10793–10798. doi:10.1073/pnas.0602493103